**High Quality CT Image Reconstruction from Limited Projections Obtained from MiSpinner**

by

Huanyi Zhou

A thesis submitted to the Graduate Faculty of
Auburn University
in partial fulfillment of the
requirements for the Degree of
Master of Science

Auburn, Alabama
May 7, 2016

Keywords: CT, steepest descent algorithm, ART,
Total Variation, IVIS Lumina XR, MiSpinner,

Copyright 2016 by Huanyi Zhou

Approved by

Stanley J. Reeves, Chair, Professor of Electrical and Computer Engineering
Peter Panizzi, Associate, Professor of Drug Discovery and Development
Thomas Denney, Professor of Electrical and Computer Engineering

Abstract

Computed tomography (CT) technology is widely used in the medical and industrial fields. However, a traditional CT machine costs too much for many researchers to afford it and prevents them from doing related research. To solve this problem, this paper explores the possibility of CT image reconstruction based on data from an IVIS Lumina XR machine providing X-ray projection images. Compared with traditional CT machine, it is much cheaper and widely used in animal research field. With the addition of the MiSpinner hardware that successively rotates an object through a sequence of angles, data that approximates that of a CT machine can be acquired. In this research, we begin by preprocessing the data so that it conforms to the geometry of traditional CT. Then we implement and explore various CT reconstruction algorithms to assess performance. Among the algorithms are filtered backprojection (FBP), algebraic reconstruction technique (ART), and total variation methods. The final result is satisfactory. Detail information is strengthened and artifacts caused by limited projections are removed. In addition, 3D rendering is also performed providing improvement in details of the object. This work shows the potential for using the MiSpinner hardware in the IVIS Lumina XR machine for CT research and provides an alternative choice to those people who want to do CT research economically.

**Keywords**: CT image reconstruction, steepest descent algorithm, ART, Total Variation, IVIS Lumina XR, MiSpinner

Acknowledgments

Dr. Stanley Reeves, my respected advisor, has the privilege of accepting my thanks. Not only has he spent a lot of time on my research but also directed my growth in the signal processing field step by step. Two years ago, the first time I walked into his office to ask him to be my advisor, I had no idea or any background about image processing, even MATLAB. But now I am skilled in using it and independently finish a research project. Such a huge change is closely related to my professor's help. I feel so lucky to be his student to become a qualified graduate student. I have learned a lot in both academic and life aspects from him. He is always passionate to answer any question no matter how easy or hard it is.

I also would like to thank Dr. Peter Panizzi and his research team. They provided me the chance to do this research and offered me a lot of help on data collection. Also I would like to thank Andrew Brannen specifically, for his help in 3D model rendering. And I would like to thank Dr. Thomas Denney, who taught me the basic idea about how CT works and shared his experience with biomedical image processing.

Finally I would like to thank my parents for their support, encouragement and sacrifice. Thanks to my mother's foresight, sending me to the US for further study, I have learned so many useful skills I didn't have before. Thanks to my father's hard work, supporting my study, I have been able to pay full attention to study without distraction.

Table of Contents

Abstract……...ii

Acknowledgments……..iii

Chapter 1 Introduction…….……..…….. 1

1.1 Computed Tomography……...…….…….1

1.1.1 Data Collection for CT….…….…… 1

1.1.2 Physical Problems Associated with Data Collection…….…….... 3

1.1.3 CT Scanning Mode….…….……...4

1.2 IVIS Lumina XR System…….…….....7

1.2.1 System Components……...7

1.2.2 X-ray Mode……8

1.3 3D Slicer…….…….10

Chapter 2 Reconstruction Algorithm…….12

2.1 Introduction…….……12

2.2 Backprojection…….14

2.2.1 Direct Backprojection……..…….14

2.2.2 Projection Slice Theorem……..……18

2.2.3 Filtered Backprojection……...……..19

2.2.4 Convolution Backprojection …...……...…… 21

2.3 Algebraic Reconstruction Technique…….....22

2.3.1 Relaxation Method……..……...24

2.3.2 Steepest Descent Method…….……25

2.4 Total Variation for Image Recovery ……..….27

2.5 Adopted Algorithms……...….…….29

Chapter 3 Experiment……32

3.1 Phantom Image …….…..32

3.2 Image Pre-processing……...33

3.3 Image Reconstruction……..34

3.4 Image Enhancement ……39

3.4.1 Interpolation……..39

3.4.2 ART Method……41

3.4.3 Total Variation denoising……45

3.5 3D Reconstruction…….....49

3.5.1 ART in 3D Mode…….49

3.5.2 Total Variation in 3D Mode……50

3.5.3 3D reconstruction……52

Chapter 4 Conclusion……...55

4.1 Conclusion……..…55

Reference……..56

# Chapter 1 Introduction

## 1.1 Computed Tomography (CT)

Computed Tomography, known as CT scan, is an advanced technique used for producing cross-sectional images of an object based on its X-ray scan images taken from different angles, allowing the user to see inside information of the object without cutting.[1]

Traditional X-ray technique can only provide object's projection image. If there exists some overlap in the projection path, the image is blur and the objects are undistinguishable. To solve that problem, CT aims to reconstruct a cross-sectional image of the object. It sends a narrow X-ray beam passing through the object from X-ray source and sets a detector on the other side to detect the intensity. Then, the source and detector's position are changed and measurement is repeated. Compared to the original intensity, CT technique could find out the loss of X-ray beam which records the attenuation information. Once obtained all attenuation information in every direction around the body, based on some algorithms, CT technique can reconstruct the cross-sectional image.

Detected X-ray beam intensity is called projection, and the process of producing cross-sectional images is called image reconstruction from projections.

### 1.1.1 Data Collection for CT

Image reconstruction technique was proposed in 1963 and it has repeatedly arisen in a large number of scientific, medical, and technical fields in recent years for its amazing property, providing inside information of an object without harming it.[2] Especially in the diagnostic

medicine field, CT has revolutionized the radiology field. Its general idea is measuring the attenuation of X-rays along a large number of lines through the human body, and then reconstructing the slice images based on the Radon Transform. Each of those data measurements is related to a source and a detector.

For each combination of source and detector, two measurements are taken: calibration measurement and actual measurement. This is seen in Fig 1.1.

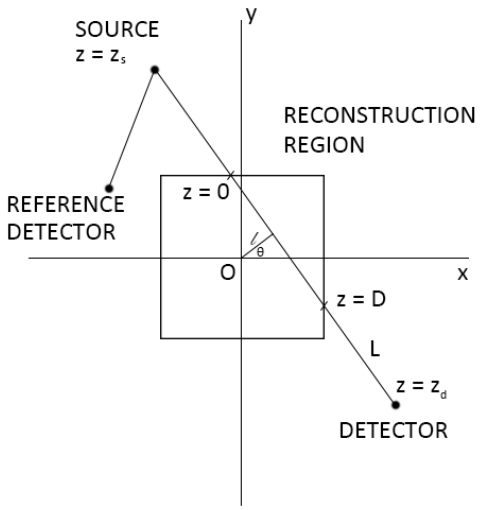


Fig 1.1 Data collection for CT (Illustration provided from Image book Reconstruction from Projections)

During the calibration measurement, our object of interest is not in the reconstruction region. The X-ray beam, from the source to the detector, traverses through a homogeneous reference material, air or water for example. This measurement can tell us the number of photons counted by the detector affected by environment.

During the actual measurement, the object of interest is inserted into the reconstruction region. The procedure of actual measurement is defined the same as the calibration measurement, but this measurement counts the number of photons that traverse through the object affected by the absorbing and scattering properties.

With these two measurements, some effects caused by external environments can be removed using relative linear attenuation coefficients, also known as CT number, to obtain a relative clear reconstruction image. However, there are still some physical problems in measurements affecting the results that cannot be ignored.

### 1.1.2 Physical Problems Associated with Data Collection

When an X-ray beam passes through the body, its attenuation at any point is related with its energy distribution and the material at that point.[2] Theoretically, CT is willing to be considered as monochromatic for calculation and thus attenuation is only related to the material occupying the space. That is desirable for diagnostic purpose. However, in practice, CT is polychromatic composed by a variety of energy, its energy changes when passing through the object.

The problem caused by polychromatic is the beam hardening, because attenuation at a fixed point is different for beams owing different energy: the lower energy, the greater attenuation is. When an X-ray beam passes through the object, its lower energy is absorbed, higher energy is left, its spectrum changes and seems hardening. Given a fixed point inside the body, when X-ray beams come from different directions (before reaching that point, they have passed through

different materials), they have different energy and will be attenuated differently at that point, which is a problem for assigning a specific single value of attenuation coefficient at that point.

Another problem is photon statistics which is caused by the photon scatter. When photons are emitted in a unit time, some will be absorbed, some will be scattered and only some of them can finally reach the detector. We can denote this probability as P and it is referred to as the Poisson probability law.

$$P_Y(y) = \exp(-\lambda)\,\lambda^y / y! \tag{1}$$

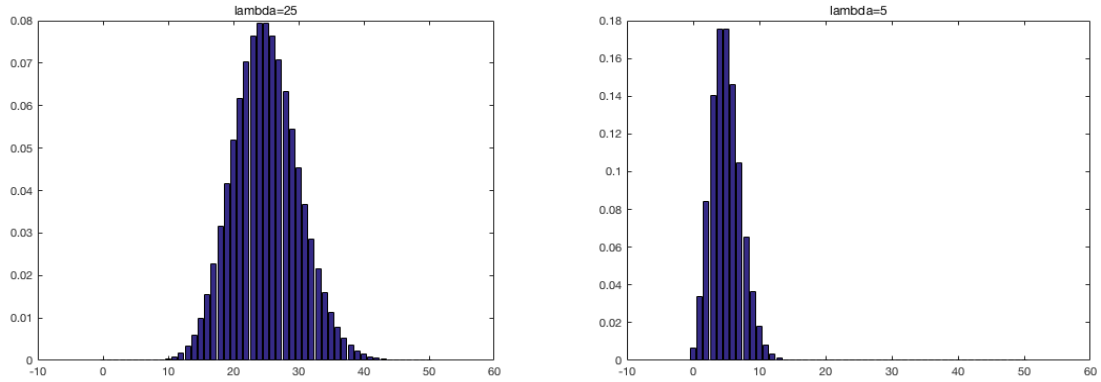


Fig 1.2 Poisson distribution with $\lambda = 5$ and $\lambda = 25$ (Illustration provided from Image Reconstruction from Projections)

There are also some other problems caused by source, detector and scanning mode used. Those problems seriously affect the accuracy of the data collection.

### 1.1.3 CT Scanning Modes

Nowadays there are many kinds of CT machine, but fundamentally, there are five basic designs used for data collection.[2]

The first scanning mode uses a single x-ray source and a single detector. There are two motions involved. First the source and the detector are moved in a parallel direction obtaining one projection sample. Then the apparatus will rotate in a small amount and do the parallel scanning again. After repetition of these two motions, projection data are collected for a large number of sets of parallel rays. This method avoids beam scatter noise and can be calibrated at the beginning of the scan. However, this method will take some time; thus, it is inappropriate for organs which cannot stay stationary, such as the lung.

The second scanning mode, trying to speed up the collection process, uses an array of detectors instead of a single detector. So when source and detectors are moved in parallel, the data are collected for several sets of parallel rays. The rotation angle can be increased to save the scanning time, and yet the total number of sets of parallel rays is still increasing. However, beam scatter in the second scanning mode is indispensable.

The third scanning mode, a more advanced design, only involves one motion. It is still a combination of single source and an array of detectors, but the array is large enough to cover the whole reconstruction region. So the rays diverge from the source to the detectors can be collected simultaneously and whole projection data can be collected by just rotating the source/detectors around the patient, which could reduce the scanning time into several seconds. Before using this scanning mode, calibration must be done carefully, to make sure in all positions the line from the source to the detector goes through the patient, then measurement will be accurate.[2]

The fourth scanning mode, an alternative fast method of data collection, uses a stationary array of detectors and a movable X-ray source moves inside in a circle. As source moves, the line from one detector to the source can form a fanbeam projection. Calibration can be adjusted at any time because at the beginning the line from the detector to the source is outside the reconstruction area. However, in this mode, it requires more detectors than the previous mode to avoid a situation where radiation goes through the body but ends up between two detectors, which is undesirable to the patient. Also, beam scatter problem is more serious than before since the direction from detector to source always changes.

Actually the first four scanning modes are inappropriate for precise imaging of a rapidly moving organ because they cost too much time for scanning compared to the organ's movement, thus, collected data at different time cannot match perfectly. So, the fifth scanning mode, designed to solve these problems, applies a totally new method for data collection. An array of X-ray sources is arranged in a semicircle and they can be electronically switched on and off.[2] So, most projection data could be collected at the same time when sources are switched on, only taking one-hundredth of a second. This scanning mode could solve the mentioned problems, but it has its own concerns. Firstly, the number of projections is limited by cost and size. Secondly, the error due to scatter occurs more frequently.

In this paper, IVIS Lumina XR system is used to collect the projection data. Its source and detectors are stationary and its shelf for placing object is movable. The projection images are obtained by rotating the object using a MiSpinner, similar to the fourth CT scan mode.

## 1.2 IVIS Lumina XR System

IVIS Lumina XR system is a high-sensitivity, in vivo imaging platform that provides the opportunity to view the inside of the body without harming it and to track cellular and genetic activity within a living organism through optical and X-ray modalities. [3]

### 1.2.1 System Components

IVIS Lumina XR system is consists of a charged coupled device(CCD) camera that can image animal subjects (primarily mice) using three modalities: bioluminescence, fluorescence and X-ray, an imaging chamber with controlling electronics, an X-ray source and detector including controls and safety systems and a Fluorescence Module including excitation and emission filters.[3] In imaging chamber, controlling electronics, MiSpinner, are consists of a 3D printed stage, an actuated motor, an animal holder, a foam insert, a cap connector and a controller, shown as Fig 1.3 a and their combination is shown as Fig 1.3 b. With the help of MiSpinner, pictures can be taken through a sequence of angles using that controller and if the system works in X-ray mode, these pictures are similar to those obtained from a CT machine.

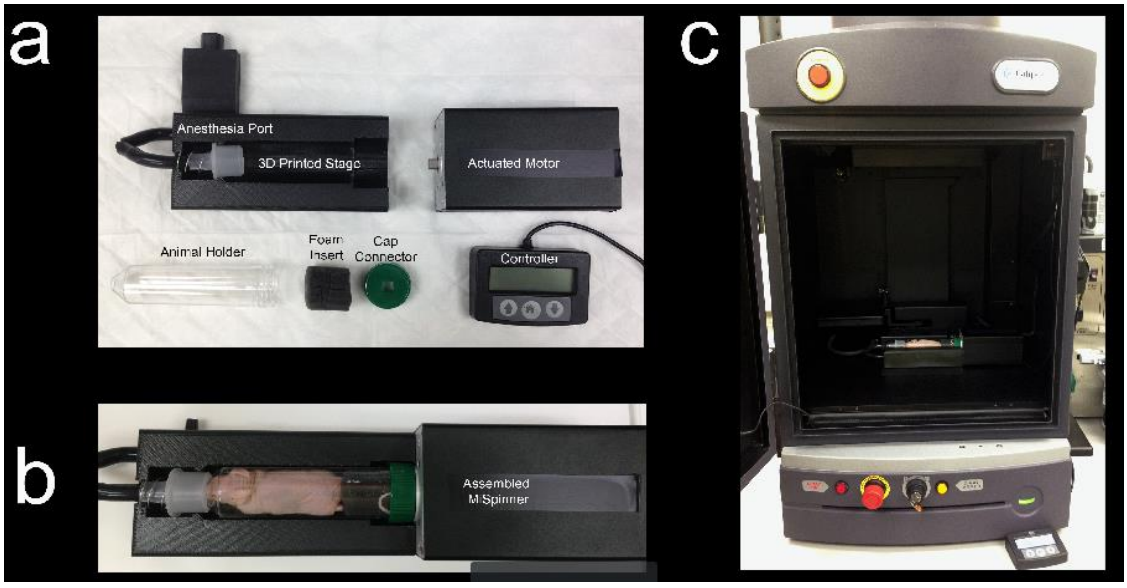

Fig 1.3 IVIS Lumina XR imaging chamber (Illustration provided by Dr. Panizzi and his research group)

Actually, IVIS Lumina XR system is just a part of the whole system, controlled by a pre-configured computer running Living Image software, shown in Fig 1.4. Except the imaging system and the computer, there is an extra light source module for fluorescence use under the imaging chamber. An XGI-8 Gas Anesthesia Delivery System provides isoflurane for anesthetizing small animal in the middle.

Fig 1.4 whole IVIS Lumina XR imaging system (Illustration provided from IVIS Lumina XR System Manual)

1.2.2 X-ray Mode

The imaging system could be simplified as Figure 1.5 when running X-ray mode. The X-ray source is located at the bottom of the system and the X-ray beam is directed upward through the imaging chamber floor. There is a movable shelf in the chamber room placing MiSpinner and the beam will pass through the shelf and hit the scintillation plate. The CCD camera will capture the

image produced in the scintillation plate. When not in X-ray mode, the scintillation plate can be moved out.

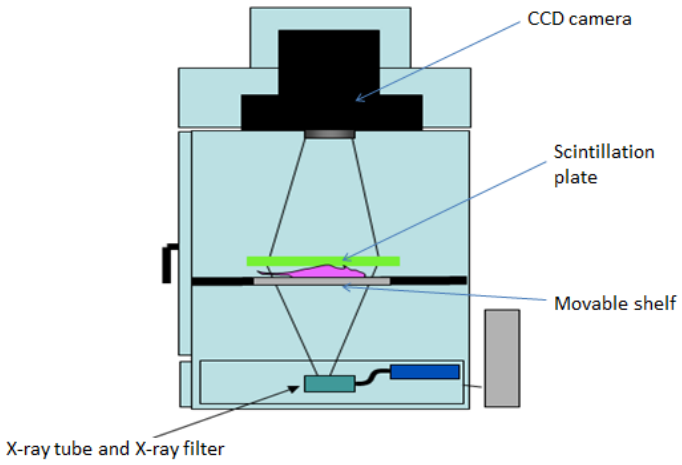


Fig 1.5 Structure of imaging system, X-ray schematic (Illustration provided from IVIS Lumina XR System Manual)

In pracitice, X-ray source and CCD camera are stationary. MiSpinner placed on the movable shelf is connected with a controller out of the chamber and its actuated motor can rotate the mice loaded tube a certain degree when controller is switched on and off once. Thus, after a series of operations, the object's total projection images can be obtained when operating the X-ray mode. However, the problem in data collection is taking each projection image will cost almost 30 to 60 seconds and totally will be about 30 minutes to an hour depending on the number of projections. To a live animal, this is a plenty long time that the effects caused by its breath and unconscious movement are not ignorable. And these effects can be seen clearly in the obtained images, shown in Figure 1.5. Better results will likely be obtained using dead mice instead. These will avoid effects caused by its breath and movement, but still there may be a bit of shift in projection

images caused by tube rotation. For live mice more sophisticated correction techniques may be necessary to get useful results.

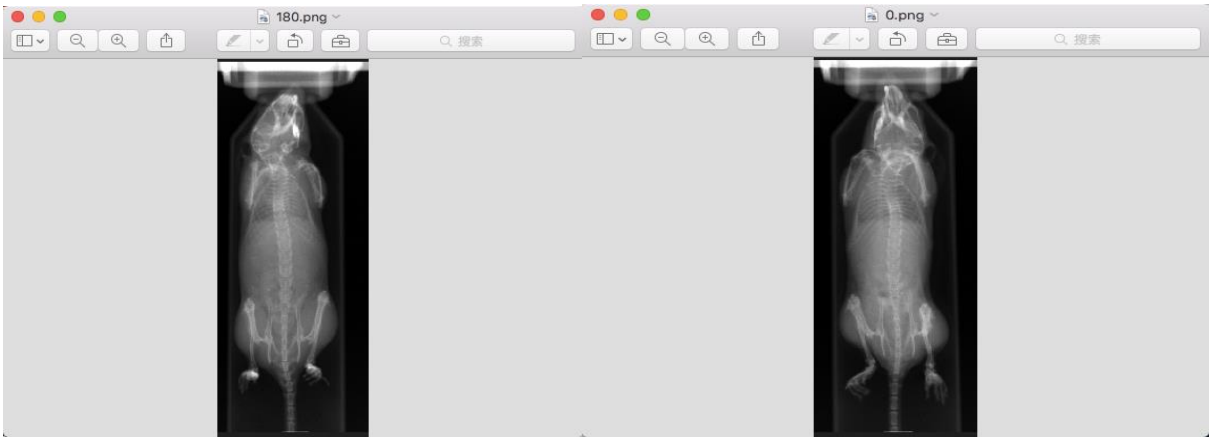


Fig 1.5 Mouse X-ray images from MiSpinner, left is taken at 180 degree, right is taken at 0 degree (Illustration provided by Dr. Panizzi and his research group)

From Fig 1.5, we can see the mouse in the left image is a bit more swollen than the right one at the lung part, which may be caused by the breath of the mouse, and we can see there is some difference at the feet side, which may be caused by the movement of the mouse. Thus, to avoid these effects, we use a dead mouse for data collection in the real situation and a wire for calibration.

## 1.3 3D Slicer

3D Slicer is a free and open source software package for image analysis and scientific visualization.[4] In this paper, 3D slicer is used for 3D reconstruction. It could provide front view, left view and vertical view of an object and a reconstructed 3D model based on those three views. What's more, in this software, it provides many 3D models for direct 3D reconstruction.

Take CT reconstruction for example, it provides CT-bone structure, CT-air structure, CT-abdomen view, CT-brain view and CT-lung view functions. Users can set a threshold value for displaying details, removing undesirable noise, increasing contrast, to present a better 3D model. Since it provides powerful functions in 3D reconstruction, especially in medical field, it is a great tool to visualize 3D reconstructions in this paper.

Chapter 2 Reconstruction Algorithm

2.1 Introduction

The major purpose of reconstruction algorithm is to figure out the distribution of the attenuation coefficients, known as CT numbers, in the image. Before calculating those coefficients, some assumptions are needed: (1) slices are infinitely thin; (2) all X-ray photons travel in the same straight line. Then, the distribution of the CT numbers among the objects can represent the distribution of the grayness in the reconstructed image.

The basic idea of image reconstruction can be seen in Fig 2.1. Assume original intensity of the X-ray beam is $I_0$, detected intensity is I, attenuation coefficient is μ.

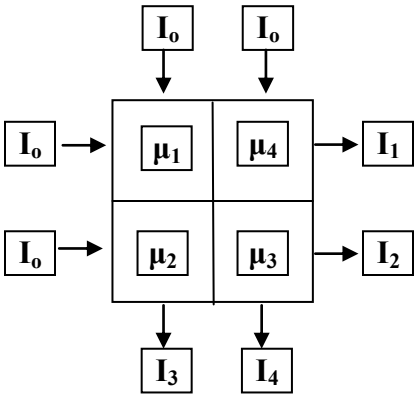


Fig 2.1 a concept map of projection

In the Fig 2.1, there are four parts in the middle region, which represent four unknown coefficients, $\mu_1$, $\mu_2$, $\mu_3$, $\mu_4$. Also there are four paths for X-ray beam passing through the middle region both in horizontal and vertical directions, thus, we can measure four intensities, $I_1$, $I_2$, $I_3$, $I_4$. Then, we can obtain four equations.

$$I_1 = I_0 e^{-(\mu_1+\mu_4)d} \qquad (2)$$

$$I_2 = I_0 e^{-(\mu_2+\mu_3)d}$$

$$I_3 = I_0 e^{-(\mu_1+\mu_2)d}$$

$$I_4 = I_0 e^{-(\mu_4+\mu_3)d}$$

Theoretically, once have four equations and four variables, the equations are solvable, which means the density of the attenuation coefficients could be calculated out. Then the image can be reconstructed based on that. This is the basic idea of image reconstruction from projections.

However, in practice, the whole process is more complicated. The reconstruction region is more than a 2×2 image; it is consists of thousands of pixels. And the attenuation coefficient is not just the sum of two elements; it is an integral along the X-ray path, shown in Fig 1.1.

$$m \simeq \int_0^D \mu_s(x,y) d_z \tag{3}$$

Since the attenuation out of the reconstruction region is 0, the length of integration is along the object. Then image reconstruction problem attempts to estimate all attenuation coefficients based on those integrals along a number of lines.

This problem theoretically was solved by Radon in 1917. Radon proved that[2,5]

$$\mu_s(x,y) = -\frac{1}{2\pi^2} \lim_{\varepsilon\to\infty} \int_\varepsilon^\infty \frac{1}{q} \int_0^{2\pi} m_1(x\cos\theta + y\sin\theta + q, \theta)\, d\theta dq \tag{4}$$

Where $m_1(l,\theta)$ denotes the partial derivative of $m(l,\theta)$. It seems in 1917, CT image reconstruction problem was solved. However, his formula has some practical difficulties in applying it:

(a) Radon's formula requires infinite line integrals to obtain the image; however, in CT image reconstruction, there are only a finite set of measurements.

(b) The projection data we obtained is affected by beam hardening, photon scatter, X-ray beam width and so on noise. Radon's inversion formula is sensitive to these effects.

(c) Radon's formula is a mathematical solution, involving a lot of calculation. If we want to use a computer for calculation, we need an algorithm to realize it.

Thus, in such a limited situation, the development of image reconstruction algorithm from limited projection data has been necessary.[6]

## 2.2 Backprojection

### 2.2.1 Direct Backprojection

Backprojection is one of the basic algorithms to explore the image reconstruction. At the very beginning, people use direct backprojection method to reconstruct image.[7] Backprojection smear the projections back across the image and adds them together to recover the image. Fig 2.2 is an example of the direct backprojection method.

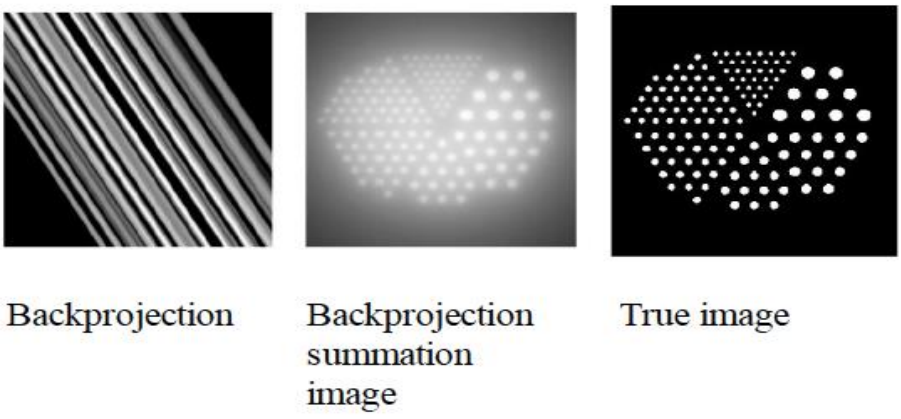


Fig 2.2 an example of direct backprojection application (Illustration provided from Computed Imaging Process Course by Dr. Denney)

Obviously, this method is inaccurate. The reconstructed image obviously is much blurrier than the true one. It is consists of a series of straight lines. A more specific explanation is shown in Fig 2.3.

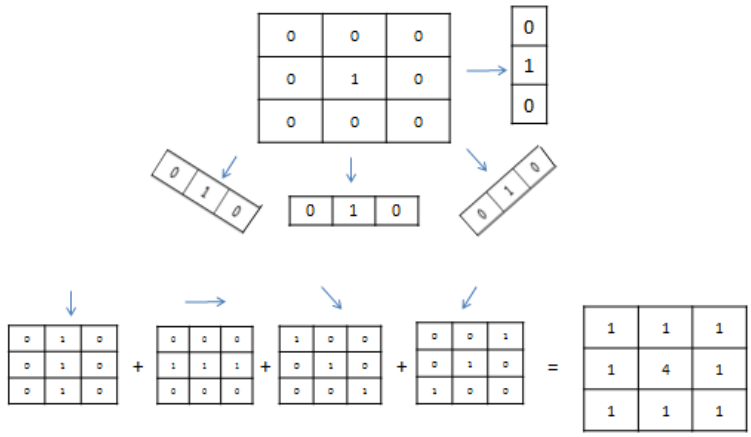


Fig 2.3 an explanation of direct backprojection method (Illustration provided from Imaging System in Medicine)

From Fig 2.3, we can find that the pattern of reconstructed image is similar to the original image, but its center point density is much higher than the normal value, and also there are some unexpected values appearing. That's why there is a cloud shadow around the objects in the backprojection summation image in Fig 2.2. It is a good first effort to reconstruct the image, although its result is not satisfactory.

To reduce those cloud shadows, some mathematical calculation is needed. Assume projection angle is $\theta$, its projection value is $g(R,\theta)$, shown in Fig 2.4. Then based on direct backprojection method, the density of attenuation coefficients along the projection theta is

$$b_\theta(x,y) = \int_{-\infty}^{+\infty} \mathrm{g(R,\theta)}\delta(x\cos\theta + y\sin\theta - R)\, dR \tag{5}$$

Where $b_\theta(x,y)$ stands for the attenuation coefficients.

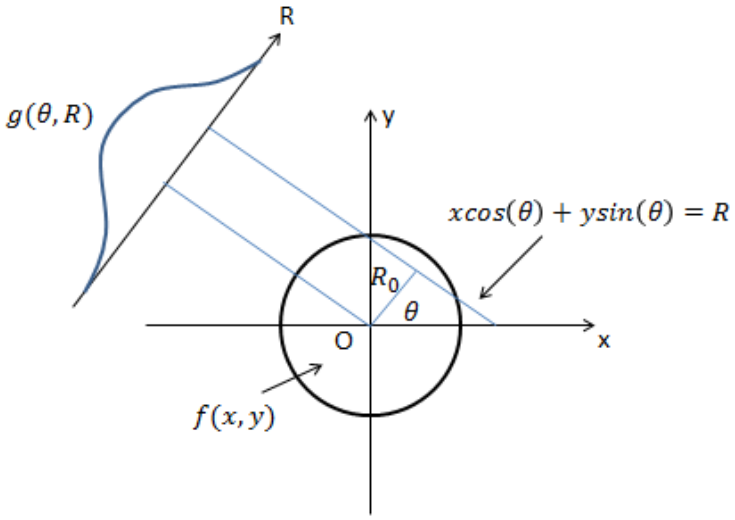


Fig 2.4 sketch map of one projection (Illustration provided from Imaging System in Medicine)

Given a straight line $x\cos\theta + y\sin\theta = R_0$, any point($x_0$, $y_0$) on this line is described by the equation

$$\begin{aligned} b_\theta(x_0,y_0) &= \int \mathrm{g(R,\theta)}\delta(x_0\cos\theta + y_0\sin\theta - R)\, d \\ &= \mathrm{g}(x_0\cos\theta + y_0\sin\theta, \theta) \\ &= \mathrm{g}(R_0, \theta) \end{aligned} \tag{6}$$

Then adding all results, the density of attenuation coefficients of reconstructed image $f_b(x,y)$ is

$$f_b(x,y) = \int_0^\pi b_\theta(x,y)d\theta \tag{7}$$

$$= \int_0^{\pi} d\theta \int_{-\infty}^{+\infty} \mathrm{g(R,\theta)}\, \delta(x\cos\theta + y\sin\theta - R)dR$$

Looking at Fig 2.2 and Fig 2.3, $f_b(x,y)$ is different from the original density $f(x,y)$. To obtain $f(x,y)$, we need to revise $f_b(x,y)$.

Assume $\mathrm{f(x,y)} = \frac{\delta(r)}{\pi|r|}$, applying polar coordinates, the projection value $g_\theta(R)$ becomes

$$\mathrm{g(R,\theta)} = \int_0^{2\pi}\int_0^{\infty} \frac{\delta(r)}{\pi|r|}\delta[r\cos(\theta-\phi)-R]r\,dr\,d\phi \tag{8}$$

$$= \int_0^{\pi}\int_{-\infty}^{+\infty} \frac{\delta(r)}{\pi|r|}\delta[r\cos(\theta-\phi)-R]r\,dr\,d\phi$$

$$= \int_0^{\pi} \frac{\delta(R)}{\pi} d\phi \quad = \delta(R)$$

$f_b(x,y)$ becomes an impulse response function $h_b(r)$

$$h_b(r) = \int_0^{\pi} d\theta \int_{-\infty}^{+\infty} \delta(R)\,\delta[r\cos(\theta-\phi)-R]dR \tag{9}$$

$$= \int_0^{\pi} \delta[r\cos(\theta-\phi)]d\theta$$

$$= \int_0^{\pi} \frac{\delta\left[\theta - (\frac{\pi}{2}+\phi)\right]}{\frac{\partial}{\partial\theta}\mathrm{r}\cos(\theta-\phi)} d\theta$$

$$= \frac{1}{r}$$

We can see the relationship between the $f_b(x,y)$ and $\mathrm{f(x,y)}$ is

$$f_b(x,y) = \mathrm{f(x,y)} ** \frac{1}{r} \tag{10}$$

where ** stands for convolution calculation.

The operator 1/r is the reason that leads to the cloud shadow in the reconstructed image. Hence, if we want to improve the image, one possible solution is using the Fourier transform, the equation becomes

$$F_b(\rho,\beta) = F(\rho,\beta)\frac{1}{\rho} \tag{11}$$

where functions $F_b(\rho,\beta)$ and $F(\rho,\beta)$ are the Fourier transform of the functions $f_b(x,y)$ and $f(x,y)$. If we can put a corresponding operator $\rho$ on the both sides, and then do the inverse Fourier transform, theoretically we can obtain the original density $f(x,y)$ in the end. But the problem is this method requires a lot of projections and the acquisition process takes a lot of time.

### 2.2.2 Projection Slice Theorem

The Fourier transform is employed in another method called the Projection Slice Theorem.

Considering two dimensional Radon transform:

$$\mathrm{g(R,\theta)} = \iint f(x,y)\delta(x\cos\theta + y\sin\theta - R)dxdy \tag{12}$$

where $\mathrm{g(R,\theta)}$ stands for the projection data, $f(x,y)$ stands for the density of attenuation coefficients, $\theta$ is projection angle and R is the line distance, seen in Fig 2.4.

Taking 1D Fourier transform of both sides of R, denoted as ρ, then

$$\begin{aligned} \mathrm{G(\rho,\theta)} &= \mathrm{F\{\, g(R,\theta)\,\}} \\ &= \int_{-\infty}^{+\infty} g(R,\theta)e^{-2\pi j\rho R}\,dR \\ &= \int_{-\infty}^{+\infty}\left[\iint_{-\infty}^{+\infty} f(x,y)\delta(x\cos\theta + y\sin\theta - R)dxdy\right]e^{-j2\pi\rho R}\,\mathrm{dR} \end{aligned} \tag{13}$$

According to sifting property, $\mathrm{R} = \mathrm{x}\cos\theta + y\sin\theta$

$$\mathrm{G}(\rho,\theta) = \iint f(x,y)e^{-j2\pi\rho\,(x\cos\theta + y\sin\theta)}dxdy \tag{14}$$

$$= \mathrm{F}\{\mathrm{f}(\mathrm{x},\mathrm{y})\}\big|_{v=\rho\sin\theta}^{\mu=\rho\cos\theta}$$

$$= F(\mu,v)$$

The one dimensional Fourier transform of projection data $\mathrm{G}(\rho,\theta)$ equals to the two dimensional Fourier transform of density coefficients $F(\mu,v)$.

Thus, the basic procedure of image reconstruction using PST is:

(1) take the 1D FFT of each projection

(2) use the PST to transform into 2D Fourier transform

(3) Interpolate those data onto a regularly-spaced grid

(4) take inverse FFT to obtain the density of attenuation coefficients

Theoretically PST method could provide accurate result, but the problem is interpolation costs a lot of time.

2.2.3 Filtered Backprojection

An improved method is called filtered backprojection. To avoid the interpolation in the PST method, filtered backprojection inverses the Fourier Transform first, and then smears back across the image like direct backprojection method.

Given 2D Inverse Fourier Transform equation

$$f(x,y) = \int_{-\infty}^{+\infty} \int_{-\infty}^{+\infty} F(\mu,v) e^{2\pi(\mu x + vy)} \, d\mu dv \tag{15}$$

the density of attenuation coefficients $f(x,y)$ could be obtained from its Fourier frequency components.

From the equation (14), we can obtain the Fourier frequency components of $f(x,y)$. Then according to the 2D IFT equation, we can obtain the f(x,y), for simplify, applying polar coordinate system

$$\begin{aligned} f(x,y) &= \int_0^{2\pi} \int_0^{\infty} F(\rho,\theta) e^{2\pi j\rho(x\cos\theta + y\sin\theta)} \rho d\rho d\theta \\ &= \int_0^{\pi} d\theta \int_{-\infty}^{+\infty} F(\rho,\theta) e^{2\pi j\rho(x\cos\theta + y\sin\theta)} |\rho| d\rho \end{aligned} \tag{16}$$

Re-write the $f(x,y)$ in the forms like

$$\begin{aligned} \mathrm{f(x,y)} &= \int_0^{\pi} \int_{-\infty}^{+\infty} F(\rho,\theta) |\rho| e^{2\pi j\rho(x\cos\theta + y\sin\theta)} d\rho d\theta \\ &= \int_0^{\pi} d\theta \int_{-\infty}^{+\infty} \left[ \int_{-\infty}^{+\infty} F(\rho,\theta) |\rho| e^{2\pi j\rho} d\rho \right] \delta(x\cos\beta + y\sin\beta - R) dR \\ &= \int_0^{\pi} d\theta \int_{-\infty}^{+\infty} g'(R,\theta) \delta(x\cos\beta + y\sin\beta - R) dR \end{aligned} \tag{17}$$

It is similar to the equation (7) in the 2.2.1 part, if we set a new projection data $g'(R,\theta)$

$$g'(R,\theta) = \int_{-\infty}^{+\infty} F(\rho,\theta) |\rho| e^{2\pi j\rho R} d\rho \tag{18}$$

Hence, if we can revise the projection data $\mathrm{g(R,\theta)}$ to $g'(R,\theta)$ by timing an operator $|\rho|$ in the frequency domain, we can obtain the original attenuation density $f(x,y)$ and reconstruct the image using direct backprojection method.

The basic procedure is:

(1) take the 1D Fourier transform of projection data

(2) multiply the operator in the frequency domain

(3) take the inverse Fourier transform of the result of Step 2

(4) smear back across the image

(5) loop the procedure to all projection data

2.2.4 Convolution Backprojection

Convolution backprojection method is an alternative to the filtered backprojction method; they are same essentially. Equation (18) could re-write like

$$F_1^{-1}[F_1\{g(R,\theta)\}|\rho|] = g(R,\theta) * F_1^{-1}\{|\rho|\} \tag{19}$$

The difference is convolution backprojection method uses a convolution calculation in space domain to replace the FT and IFT calculation in frequency domain. It simplifies the calculation and we can still get the revised projection data $g'(R,\theta)$ and obtain the original density $f(x,y)$.

Assume function C(R) is the inverse Fourier Transform of the operator $|\rho|$,

$$C(R) = F^{-1}\{|\rho|\} \tag{20}$$

then

$$f(x,y) = \int_0^{\pi} d\theta \int_{-\infty}^{+\infty} \{g(R,\theta) * C(R)\}\delta(x\cos\beta + y\sin\beta - R)dR \tag{21}$$

However, a big problem is theoretically there is no inverse Fourier Transform of operator $|\rho|$ because the function $|\rho|$ is non-integrable. Hence, if we want to continue using this method, a solution is to find an approximate function to replace the C(R) or adding a window function on it, and that is where many researchers focus.[6~8] Some famous filter functions like R-L window

function, S-L window function and Hamming window function are widely used in the image reconstruction field.

## 2.3 Algebraic Reconstruction Technique

Algebraic Reconstruction Technique (ART) is another kind of method to reconstruct the image, including a lot of reconstruction algorithms. All of them are iterative procedures.

Assume we have an object and it is divided into n×n cells, shown in Fig 2.5, the attenuation coefficient of every cell is $x_j$, i stands for the row number from 1 to M and k stands for column number from 1 to N. Then, the attenuation equation at row i could be written as

$$x_1 + x_2 + \cdots + x_k = b_i \tag{22}$$

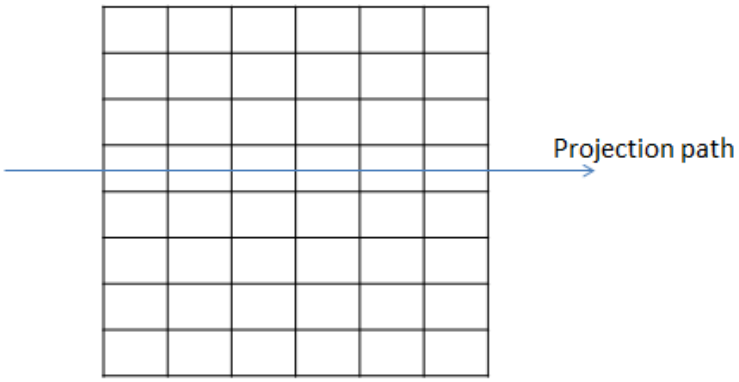


Fig 2.5 a concept map of discretization

To any projection path from the source to the detector, its attenuation equation could be

$$a_{i1}x_1 + a_{i2}x_2 + \cdots + a_{iN}x_N = b_i, i = 1,2, \ldots, \mathrm{M} \tag{23}$$

$$a_{ij} = \begin{cases} 1, & in\ the\ path \\ 0, & otherwise \end{cases}$$

Equation (24) could be simplified as

$$\sum_1^N a_{ij}x_j = b_i, i = 1,2,\cdots,M \tag{24}$$

Considering the noise or error, then the equation could be

$$\mathrm{Ax} + \mathrm{e} = \mathrm{b} \tag{25}$$

where $A = (a_{ij})_{M*N}$ is a matrix, x is wanted image vector and b is an attenuation vector calculated from the projection.

If we can solve the equation, we can reconstruct the image. However, there are several problems, (1) we have M×N variables but not so many equations, limited by the projections, (2) noise or error is hard to incorporate in the equation. Thus, equation (25) can't be solved directly and ART method is applied to solve this problem.

The basic procedure is

(1) set an initial vector of x

(2) calculate the result and compare with the attenuation vector

(3) revise the vector x based on the difference

(4) repeat those procedures until reaching the error range

That is, ART will produce a sequence of vectors $x^0$, $x^1$, $x^2$… until it converges to x*, where x* is the required estimate. $x^{(k+1)}$ is obtained from the $x^k$, matrix A and attenuation vector b.

$$x^{(k+1)} = \alpha_k(x^k, A_{ik}, b_{ik}) \tag{26}$$

$\alpha_k$ is a function of iteration number. Various ART methods differ from each other in the way the sequence of $\alpha_k$'s chosen.[2]

2.3.1 Relaxation Method

In equation (25), due to the existence of e, Ax is smaller than vector b.

$$(\alpha_i, \mathrm{x}) \leq \mathrm{b}, 1 \leq \mathrm{i} \leq \mathrm{M} \tag{27}$$

( , ) denotes the inner product of two vectors.

Set

$$N_i = \{x | (\alpha_i, \mathrm{x}) \leq b_i\}, 1 \leq \mathrm{i} \leq \mathrm{M} \tag{28}$$

$$\mathrm{N} = \bigcap_{i=1}^{M} N_i \tag{29}$$

Ni is the set of vectors which satisfies the ith of the M inequalities and N satisfies all the M inequalities. The relaxation method attempts to find an element of N.

A general way of using ART to solve the inequalities is

(1) assume $x^0$ is an arbitrary initial vector

(2) update the solution as

$$x^{(k+1)} = \begin{cases} x^{(k)}, \\ x^{(k)} + \lambda^{(k)} \frac{b_{i_k} - (\alpha_{i_k}, x^{(k)})}{\|\alpha_i\|^2} \alpha_{i_k} \end{cases} \tag{30}$$

where $\lambda^{(k)}$ is a real number as relaxation parameter, i(k)=k(mod M)+1.

If relaxation parameter satisfies

$$0 < \varepsilon_1 \leq \lambda^{(\kappa)} \leq \varepsilon_2 < 2 \tag{31}$$

Then we can prove that vectors $x^0$, $x^1$, $x^2$…derived from the relaxation method converge to a vector in N, only N is not empty. And the proof is shown in reference [2] chapter 11. If there are multiple solutions, then there must be a solution $x_{min}$, for any solution x, $||\mathrm{x}|| > ||x_{min}||$, $||\mathrm{x}||^2 = (x, x)$.

2.3.2 Steepest Decent Method

An alternative ART method is called steepest descent method, It is a first-order optimization algorithm designed to find the local minimum of a function, also known as gradient descent method.[9] Its definition is, given point a, if a real function f(x) is defined and differentiable, then f(x) decreases fastest in the direction of $-\nabla \mathrm{f}(\mathrm{x})$ at point a, shown in Fig 2.6.

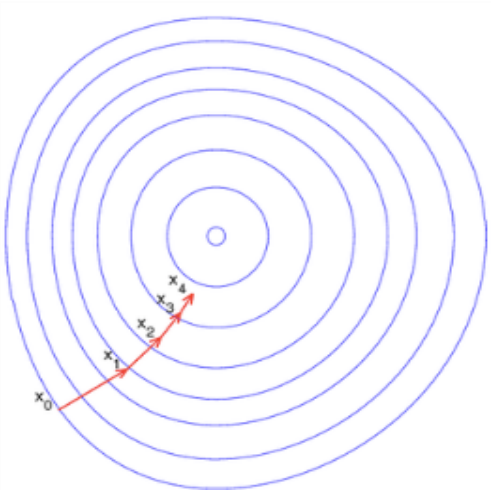


Fig 2.6 a concept map of steepest descent algorithm (Illustration from Wikipedia, “Gradient Descent”)

In Fig 2.6, function f is a bowl shape image. The blue curves stands for the constant values in function f. The red arrow is the direction of the negative gradient at that point; it is orthogonal to the curves going through that point. From the picture, we can see that the gradient descent leads the function to the bottom of the bowl, where the minimum value is found. For example, if $\mathrm{b} = \mathrm{a} - \gamma \nabla \mathrm{f}(\mathrm{a})$ , then

$$\mathrm{f}(\mathrm{a}) \geq \mathrm{f}(\mathrm{b}) \tag{32}$$

$\gamma$ is called step size and it is allowed to change at every iteration. If we choose particular values of $\gamma$ in each iteration, then we can converge the function to its local minimum value.

In image processing, steepest descent method can be used to minimize the noise or error in the image.

Set $x^{n+1} = x^n - \gamma_n \nabla f(x^n), n \geq 0$, then

$$\mathrm{f}(x^0) \geq \mathrm{f}(x^1) \geq \mathrm{f}(x^2) \geq \mathrm{f}(x^3) \ldots \tag{33}$$

Set

$$\begin{aligned} f(x) &= \|b - Ax\|^2 \\ &= (\mathrm{b} - \mathrm{Ax})^T (b - Ax) \\ &= b^T b - 2x^T A^T b + x^T A^T A x \end{aligned} \tag{34}$$

Calculate the partial derivative of $\mathrm{f}(\mathrm{x})$

$$\frac{df(x)}{dx} = \begin{pmatrix} \frac{\partial f}{\partial x_1} \\ \vdots \\ \frac{\partial f}{\partial x_N} \end{pmatrix} = 2A^T A x - 2A^T b \tag{35}$$

When $\frac{df(x)}{dx} = 0$

$$A^T A x = A^T b \tag{36}$$

$f(x)$ is minimum means x is the estimated result for image reconstruction.

## 2.4 Total Variation for Image Recovery

Based on those reconstruction algorithms above, we can obtain a cross-sectional image of the object. But when projections are limited, the quality is poor no matter which kind of algorithm is used, and the existence of noise only makes the result worse. Hence, a more sophisticated image recovery technique is necessary in image processing.

In this section, we describe a signal processing method called Total Variation (TV) denoising in noise removal. It is based on the principle that signals with excessive and possibly spurious detail have high total variation; that is, the integral of the absolute gradient of the signal is high. According to this principle, reducing the total variation of the signal subject to it being a close match to the original signal, removes unwanted detail whilst preserving important details such as edges.[10,11] That is much better than the fundamental algorithm in image processing such as linear smoothing or median filtering, which will reduce the noise but at the same time smooth away the edges.

A mathematical definition of the Total Variation is, given a digital signal $y_n$

$$V(y) = \Sigma_n |y_{n+1} - y_n| \tag{37}$$

And the definition becomes given an input signal $x_n$, trying to find an approximation $y_n$, which has smaller fluctuation than $x_n$ but "close" to it.

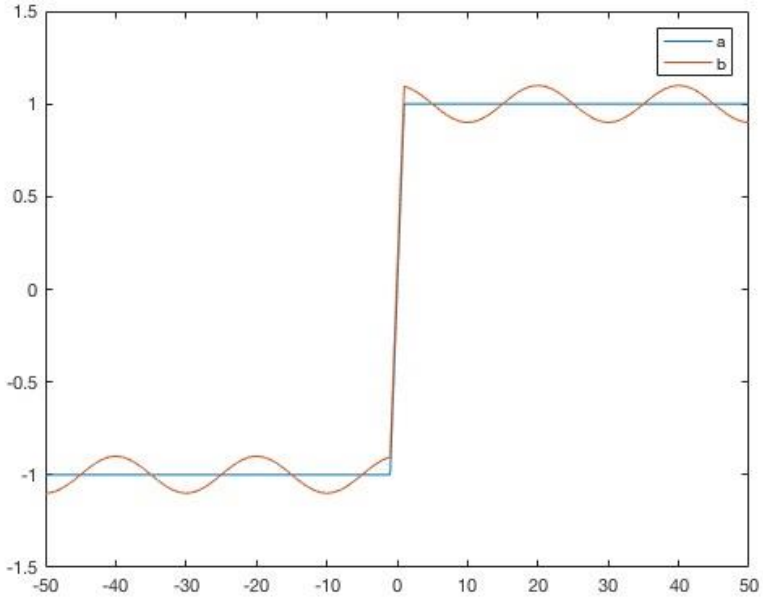


Fig 2.7 Illustration of 1D total variation

Take Fig 2.7 for example, both curve a and b represent the same information, "a" stands for the desirable signal and "b" stands for the one with noise. TV denoising is trying to find a curve, closer to "a" but with less fluctuation than "b".

Hence, one measure of closeness is

$$E(x,y) = \frac{1}{2}\sum_n (x_n - y_n)^2 \tag{38}$$

One measure of fluctuation is

$$V(y) = \sum_n |y_{n+1} - y_n| \tag{39}$$

Then a total variation denoising process could be to find the minimum value of the equation below

$$\min E(x,y) + \lambda V(y) \tag{40}$$

$\lambda$ is called the regularization parameter, and it plays an important role in the denoising problem. When $\lambda = 0$, there is no denoising and y is always identical to the x, when $\lambda \to \infty$, to make equation (40) still make sense, V(y) has to be very small, meaning there is no variation. Then y will behave like a constant and less like the input signal x, which will increase the value of $E(x,y)$. Thus, the choice of $\lambda$ is very important to achieve the best noise removal.

In image processing, given a 2D signal x, its TV norm proposed by Rudin et al. is[12]

$$V(x) = \sum_{i,j} \sqrt{|x_{i+1,j} - x_{i,j}|^2 + |x_{i,j+1} - x_{i,j}|^2} \tag{41}$$

or

$$V_{aniso}(x) = \sum_{i,j} \sqrt{|x_{i+1,j} - x_{i,j}|^2} + \sqrt{|x_{i,j+1} - x_{i,j}|^2} = \sum_{i,j} |x_{i+1,j} - x_{i,j}| + |x_{i,j+1} - x_{i,j}| \tag{42}$$

It is called $l_1$ norm, denoted as $\|\Delta(x)\|$ in this paper and Total Variation denoising form becomes

$$\min E(x,y) + \lambda V(x)$$
$$= \min \|b - Ax\|^2 + \lambda \|\Delta(x)\| \tag{43}$$

This form is much more widely seen in many papers. To solve variants of this problem, many algorithms are invented.[13~16]

## 2.5 Adopted Algorithms

In this paper, different from traditional image processing, working on a phantom image, we have 25 wire projection images and 96 mouse projection images from experiments. We use MATLAB to reconstruct a high quality cross-sectional image.

In MATLAB, there is a CT reconstruction command called iradon function which can reconstruct the image quickly and easily based on backprojection theorem, but due to the limited number of projections, the quality of reconstructed image is not satisfactory.

An improvement may be possible using the ART method. Set iradon image as initial vector $x^0$, define $\alpha_k$ function, minimize the noise vector using iteration and find the best result x. In this paper, steepest descent method is adopted and revised.

Set

$$f(x) = \|b - Ax\|^2 + \alpha||Lx||^2 \tag{44}$$

Its partial derivative is

$$\nabla f(x) = \frac{df(x)}{dx} = 2A^TAx - 2A^Tb + 2\alpha L^TLx \tag{45}$$

$$= -2A^T(b - Ax) + 2\alpha L^TLx$$

Then

$$x^{n+1} = x^n - \gamma_n \nabla f(x^n), n \geq 0, \tag{46}$$

$$= x^n + \gamma_n[2A^T(b - Ax^n) - 2\alpha L^TLx^n]$$

where b is attenuation vector, A stands for Radon transform, x is image vector, $\alpha$ is regularization parameter, L is Laplace operator, $\gamma_n$ is step size.

Normally, when $\nabla f(\mathrm{x}) = 0$, its solution x is the estimated result, but actually x is a M*N matrix, involving a lot of calculation. So, we use iteration instead of solving the equations directly, gradually approaching the solutions.

For simplicity, we set $\beta = \frac{1}{2} * \gamma_n$, then equation (46) becomes

$$x^{n+1} = x^n + \beta[A^T(b - Ax^n) - \alpha L^T L x^n] \tag{47}$$

For given $\alpha$ and $\beta$ values, we find the x that minimizes $f(x)$.

A further step is adding TV model into the steepest descent algorithm, replacing the $||Lx||^2$ part by $\|\Delta(x)\|$, image vector itself total variation.

There are many forms of total variation, based on equation (42), in this paper, we define

$$\Delta(x) = \varphi_T(x) = \begin{cases} |x| - \frac{T}{2}, & |x| > T \\ \frac{1}{2T}x^2, & |x| \le T \end{cases} \tag{48}$$

It is similar to the function |x|, but the difference is $\varphi_T$ has derivatives throughout the whole function, and its derivative is

$$\varphi_T'(x) = \begin{cases} -1, & x < T \\ \frac{1}{T}x, |x| \le T \\ 1\ , x > T \end{cases} \tag{49}$$

Then $\|\Delta(x)\|$ becomes

$$\|\Delta(x)\| = \sum_{i,j}\{\varphi_T(x_{i+1,j} - x_{i,j}) + \varphi_T(x_{i,j+1} - x_{i,j})\} \tag{50}$$

Based on equation (33), set

$$f(x) = \|b - Ax\|^2 + \alpha\|\Delta(x)\| \tag{51}$$

Then

$$\begin{aligned} x^{n+1} &= x^n - \gamma_n \nabla f(x^n), n \ge 0, \\ &= x^n + \beta[A^T(b - Ax^n) - \alpha\varphi_T'(x)] \end{aligned} \tag{52}$$

For a given choice of $\alpha$, $\beta$ and T values, find the x that minimize $f(x)$, and the estimated x is what we want to describe the inner information of an object.

Chapter 3 Experiment

3.1 Phantom Image

Before processing the actual projection data, we can run a phantom image first. The phantom image is consists of perfect data without any noise, thus, its reconstructed image could present the best result of reconstruction algorithm. In this paper, I got 25 wire projection images and 96 mouse projection images separately for image reconstruction. Phantom image reconstruction from 25 projections and 96 projections are shown in Fig 3.1.

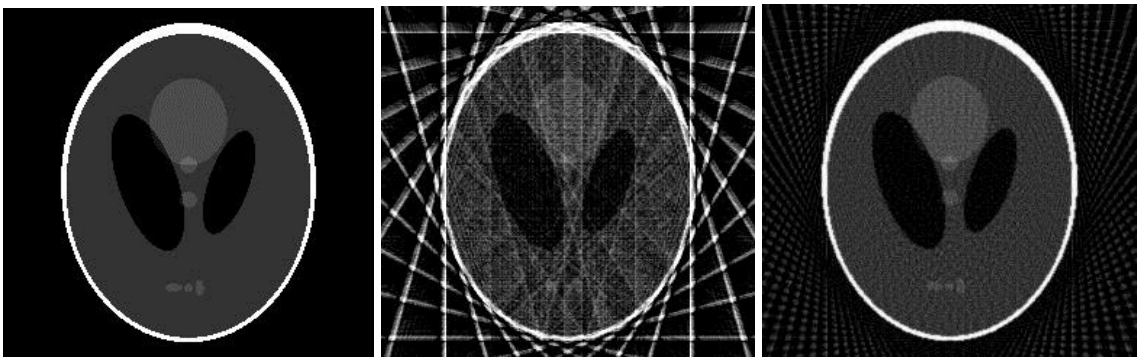

a b c

Fig 3.1 a) is a true phantom image, b) is a phantom image reconstructed from 25 projections, c) is a phantom image reconstructed from 96 projections

.From Fig 3.1, we can see that the number of projections play an important role in image reconstruction. The more projections, the better image quality is. Image c is much better than image b. Although it is hard to reach this level in actual cases, these phantom images can direct us in image processing.

3.2 Image Pre-processing

Before image reconstruction, we need to do some pre-processing work to the projections, to obtain an accurate sinogram image. A sinogram image is the basis for image reconstruction in MATLAB and it is consists of all projection images.

The original projection image from the IVIS Lumina XR is shown in Fig 3.2. The object in the tube is our interest, but we can see it is sloping clearly in the image. That is a problem for obtaining an accurate sinogram image, hence, image pre-processing is indispensable.

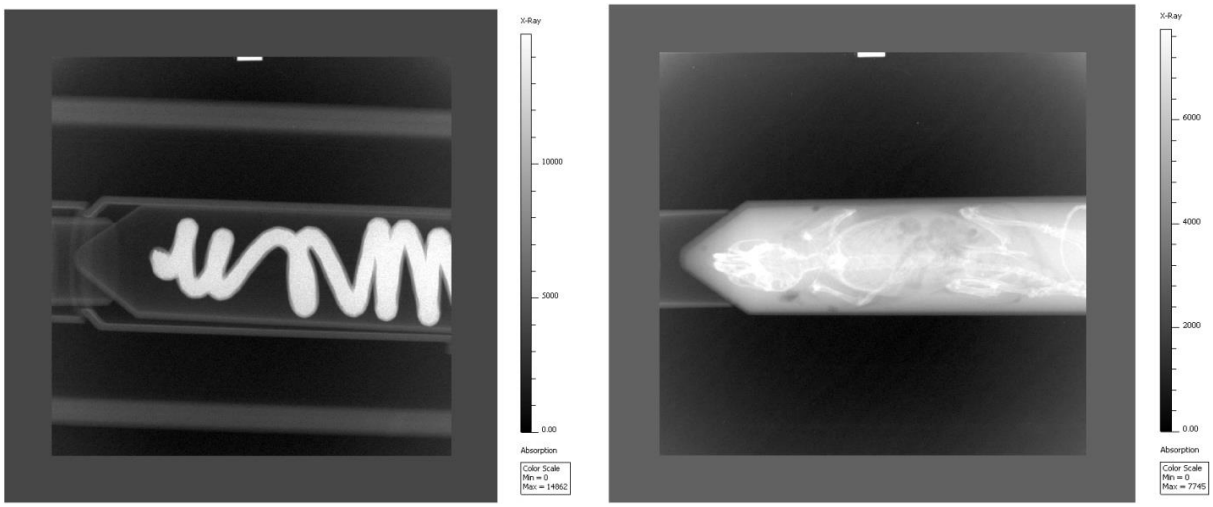


Fig 3.2 left image is an example of 25 wire projection images and right image is an example of 96 mouse projection images

In image pre-processing, the first step is to extract the middle part of the image where recording the interested information; the second step is to rotate the central axis: (1) calculating slant angle of central axis, (2) rotating the axis in order to make it flat in the horizontal direction, (3) calculating the slant angle again for a double check, if it reaches the error range, the central axis can be regarded as flat, if not, do the rotation again. (4) shifting the object into the center region. The processed image is shown below in Fig 3.3.

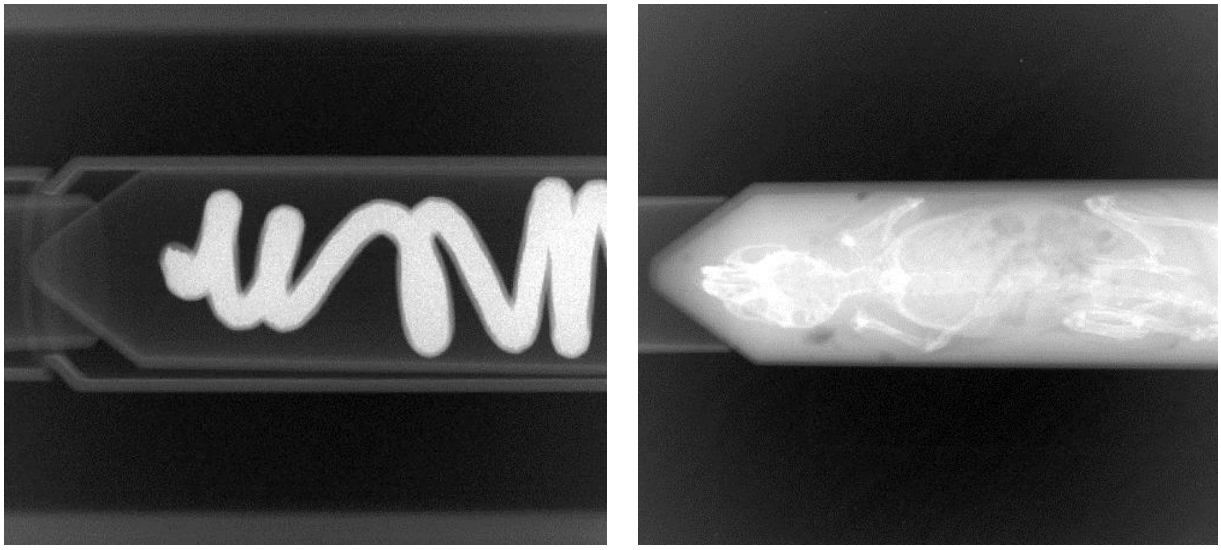

Fig 3.3 two images after image pre-processing, left is wire image, right is mouse image

Fig 3.3 shows an example of the projection images after pre-processing. The object of interest is in the center of the image, and the central axis is now flat in the horizontal direction. Then, let us concentrate on the pixels, every value of the projection images stands for an X-ray beam intensity detected by detector. With these values, we can figure out the distribution of the density of attenuation coefficients.

## 3.3 Image Reconstruction

Normally, the projection images should look like the image in Fig 3.4. When X-ray beam passes through the object, it will be absorbed or scattered by the material, thus, its intensity should be weaker than those detected out of the reconstruction region. Fig 3.4 shows the proper projection image, the outside part is brighter than the inside.

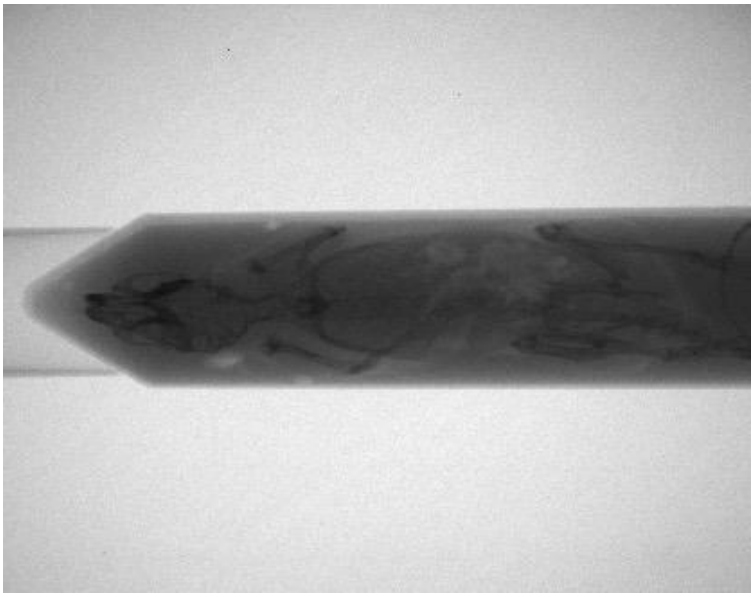

Fig 3.4 the same mouse image in Fig 3.1 in dicom format

In this project, the projection images were all in PNG format and look similar to the example in Fig 3.3. Since projection images are not in the right format, we can infer that the IVIS Lumina XR machine has done some image processing itself when producing the projection images. Based on the phenomenon it only turns dark region into bright, bright region into dark, we can guess it is a simple subtraction algorithm.

According to equation (2), projection values are

$$\mathrm{I} = I_0 e^{-\int \mu_s(x,y) d_z} \tag{53}$$

We can assume

$$\mathrm{d} = \mathrm{k} - \mathrm{I} \tag{54}$$

Where d is the value in projection images, k is a default constant as minuend, I is X-ray beam intensity, real projection value. Our aim is to calculate I for image reconstruction.

When X-ray beam passes through the object, especially high density parts, it will be seriously attenuated,$I \simeq 0$, then the corresponding place in the projection images should be very bright and its value is close to the default constant k; when X-ray beam goes through the space out of the reconstruction region, it suffers almost no loss, $I \simeq I_0$, then the corresponding place should be very dark, its value is close to the difference, k-I. So we can get the equations below

$$d_i = k - \alpha e^{-\lambda i}; \tag{55}$$

$$\lambda_i = 0;\ d_i = k - \alpha = d_{min}$$

$$\lambda_i = \infty;\ d_i = k = d_{max}$$

What we want is attenuation coefficient $\lambda_i$, its value can be obtained as

$$\lambda_i = \log\left(\frac{\alpha}{k - d_i}\right) \tag{56}$$

$$= \log\left(\frac{k - d_{min}}{k - d_i}\right)$$

$$= \log\left(\frac{d_{max} - d_{min}}{d_{max} - d_i}\right)$$

To avoid $d_{max} - d_i = 0$, we set $k = d_{max} + \varepsilon$

$$\lambda_i = \log\left(\frac{d_{max} - d_{min} + \varepsilon}{d_{max} - d_i + \varepsilon}\right) \tag{57}$$

where ε is a very small constant used to avoid error in the denominator. Data from wire projection images is more suitable for calculation, because X-ray beam could hardly pass through the wire which makes $k = d_{max}$ more precise.

Obviously, when taking the projection pictures, noise exists. Calculation will remove some evenly distributed noise, and the remaining noise does not affect the image reconstruction too much, and it will be solved by TV denoising later.

Once we obtained all attenuation coefficients, we can form a sinogram image, picking the same column in every image. That is the basis for image reconstruction and it looks like

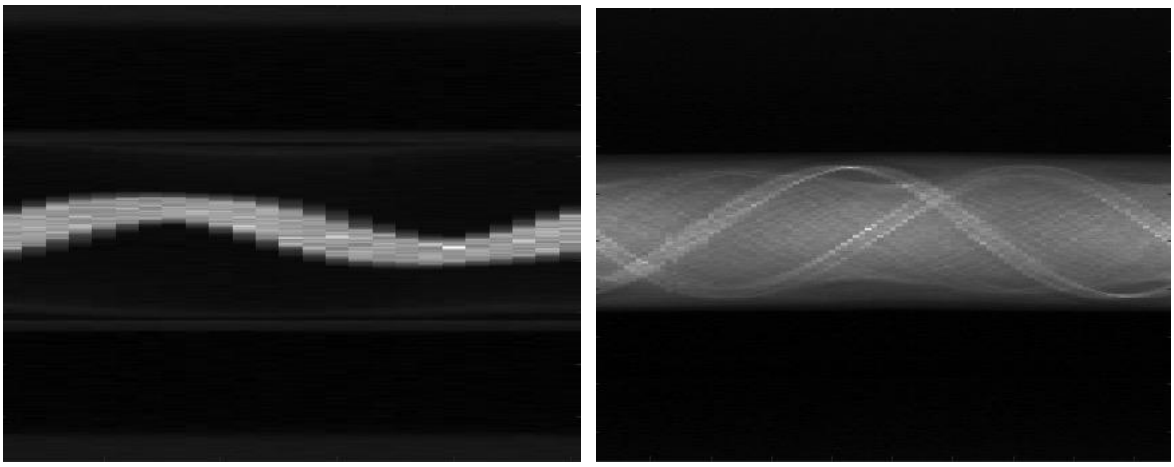

Fig 3.5 left image is a sinogram image obtained from 25 wire projections and right is a sinogram image obtained from 96 mouse projections

From the IVIS Lumina XR system manual, the size of the machine is 48cm×71cm×100cm, and the field of view in the X-ray mode is 12.5 $cm^2$, the door opening dimension is 38cm×51cm, so the distance between the shelf and CCD camera is 51 cm and the distance between the shelf and the X-ray source is 49 cm. The cone angle from the X-ray source to the shelf is 6.8 degrees along the length and 2.3 degrees along the width. Curvature of plane curves after calculating is small enough that we could regard those X-ray beams as parallel rays reaching the shelf and detected by the detector. Then we can use iradon function in MATLAB directly, and reconstructed images are shown in Fig 3.6

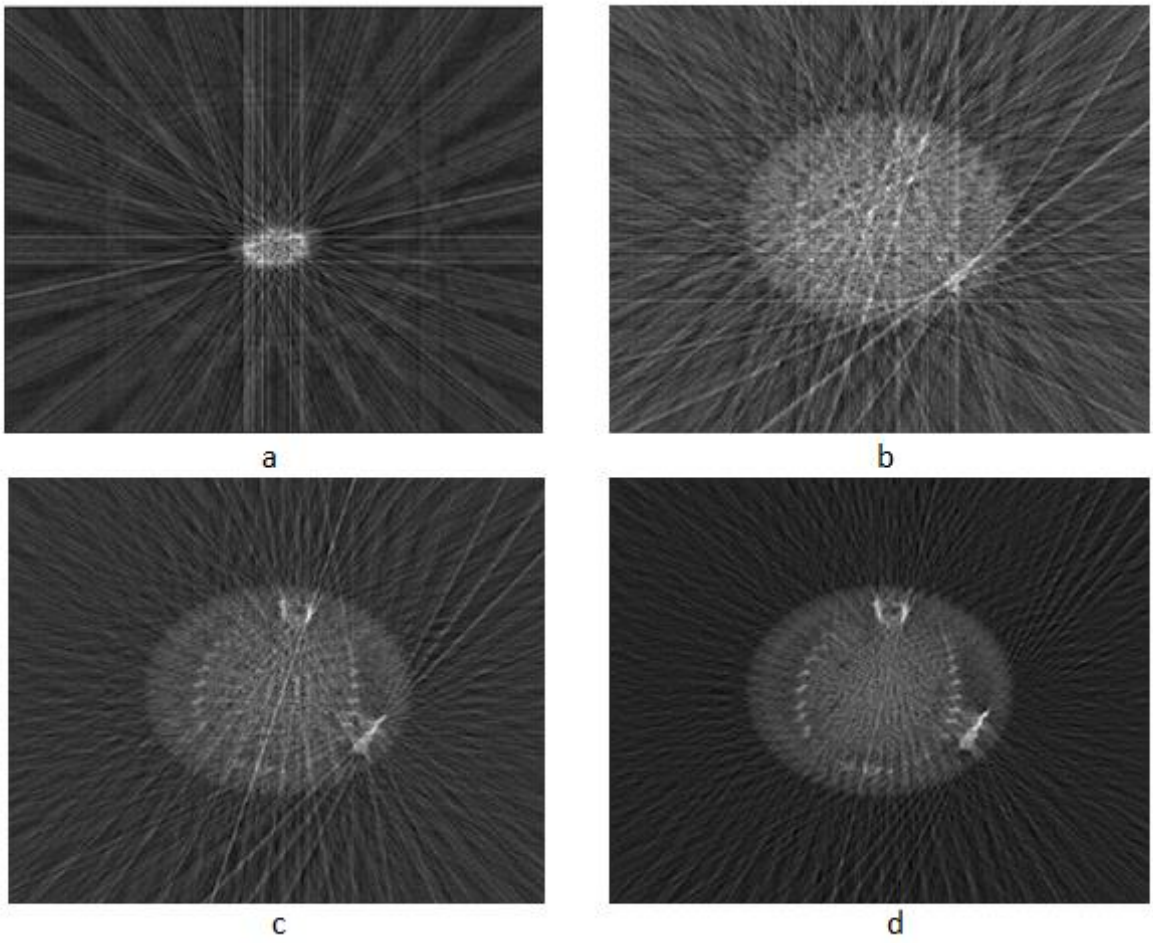


Fig 3.6 upper left image a is a slice image reconstructed from 24 wire projections, upper right image b is a slice image reconstructed from 24 mouse projections, bottom left image c is reconstructed from 48 mouse projections, bottom right image d is reconstructed from 96 projections

From Fig 3.6, we could conclude again that the number of projections plays an important role in image reconstruction. Comparing images b, c and d shows that reconstructed images can present more detail when provided more projections. And by comparing images a and b, we can see, given the same number projections, slice image from high density and simple structure object, like wire, is much easier to reconstruct than a complex object, like mouse. Image b could hardly

provide any information for a mouse. However, since the number of projections is limited, even in image d there are still many artifacts existing. We still need to do image enhancement work.

## 3.4 Image Enhancement

From digital signal processing[17], we can learn some fundamental image processing methods for noise removal.

### 3.4.1 Interpolation

Since projections play an important role in image reconstruction and its number is limited by measurement, an image processing idea is to construct extra projections artificially. In image processing, there is a method called interpolation that can enlarge information based on the known information nearby. We can use interpolation method in a sinogram image to create extra information for image reconstruction, and its result is shown in Fig 3.7

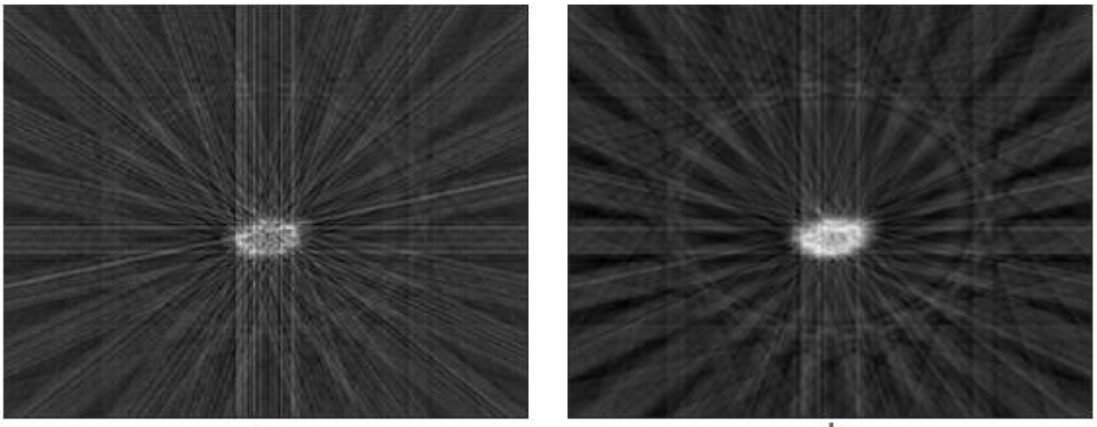

a b

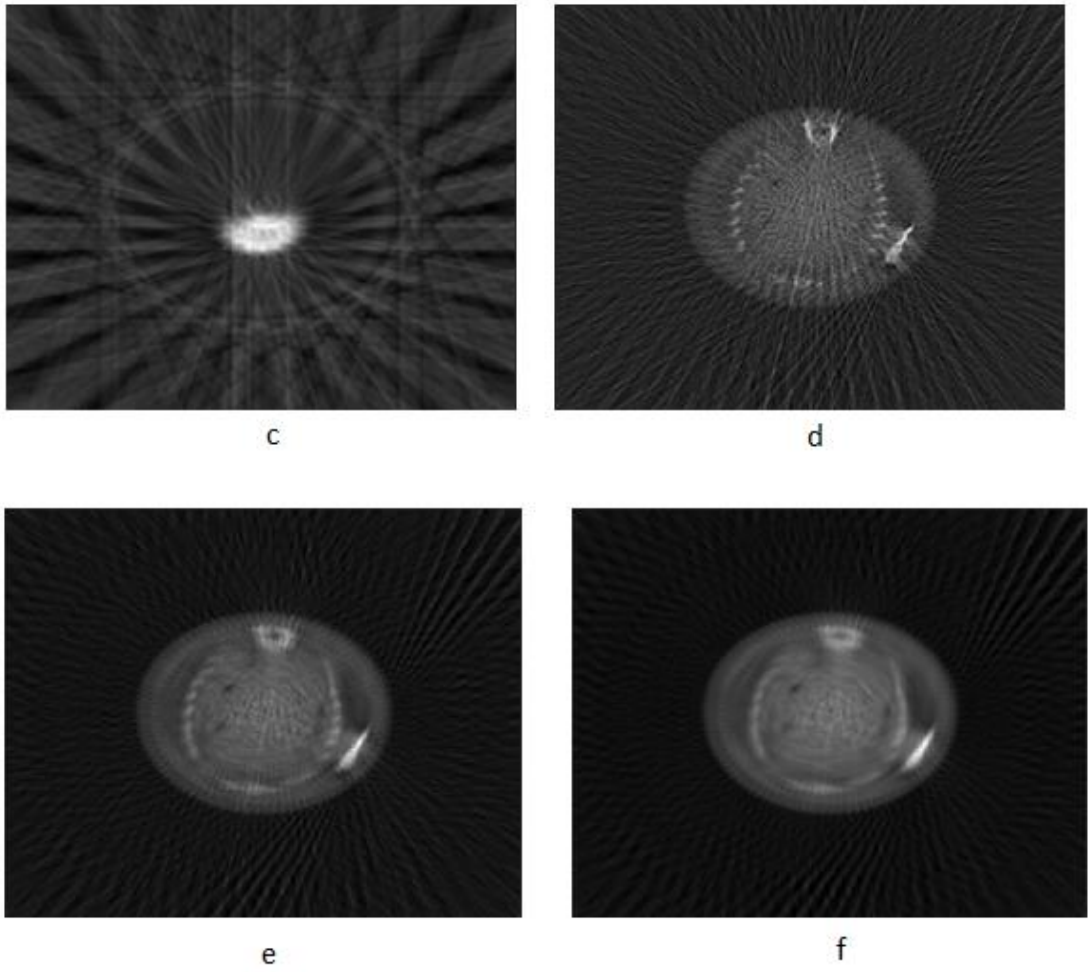


Fig 3.7 ‘a’ is original wire slice image, ‘b’ is image ‘a’ after bilinear interpolation image processing, ‘c’ is ‘a’ after bicubic interpolation image processing; ‘d’ is original mouse slice image, ‘e’ is image ‘d’ after bilinear interpolation image processing, ‘f’ is ‘d’ after bicubic interpolation image processing

Fig 3.7 shows the result of image processing after two kinds of interpolation; from the upper row, we can see that interpolation has done some work, increasing the high density part in the image. But from the bottom row, we find this method is not as good as expected. It does remove the noise around the body, but it also blurs the whole reconstructed part in the image and loses the ribs information. Hence, this image processing method is not suitable.

3.4.2 ART method

As mentioned before, ART can gradually approach the best result in reducing the noise in the image. In this paper, we have designed our own ART algorithm for image reconstruction based on steepest descent algorithm. First we set the reconstructed image from the MATLAB iradon function as initial x value in ART iteration, based on equation (47). Then we consider selecting proper $\alpha$, $\beta$ and n values to find the best x to minimize the reconstruction error.

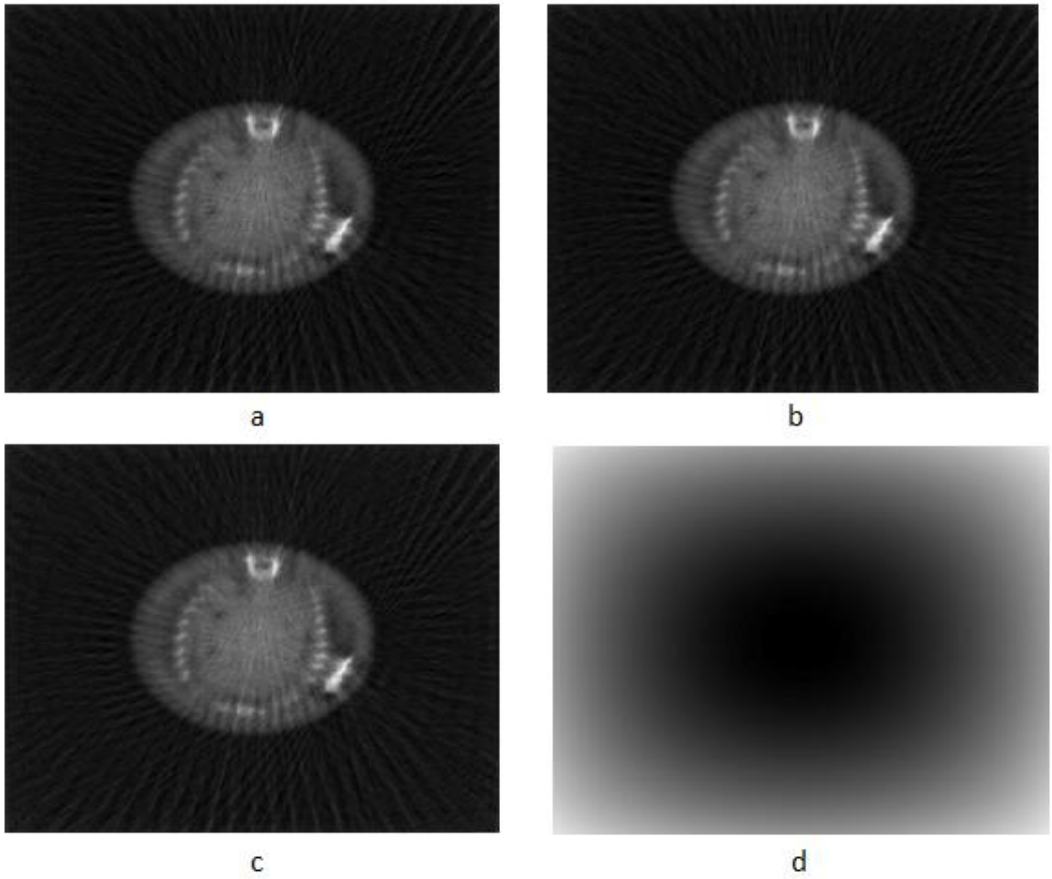


Fig 3.8 image reconstruction from projections under different $\beta$ values using ART, 500 iterations: in image a, $\alpha = 0.1, \beta = 0.001$; in image b, $\alpha = 0.1, \beta = 0.002$; in image c, $\alpha = 0.1, \beta = 0.003$; in image d, $\alpha = 0.1, \beta = 0.004$.

Fig 3.8 shows the effect of $\beta$. $\beta$ is step size parameter in steepest descent algorithm, it determines the increment size of x every iteration, it is shown as contrast in the image. If $\beta$ is too large, x will increase a lot every iteration and miss the minimum value of f(x), thus, image quality becomes worse, like image d shows; if $\beta$ is too small, x will increase a little every iteration and cannot obtain the best result in a short time. Hence, we need to find the relationship between $\beta$ value and the image quality, and pick the best value for further research. In Fig 3.8, it shows when $\beta = 0.002$, the image quality is better than others.

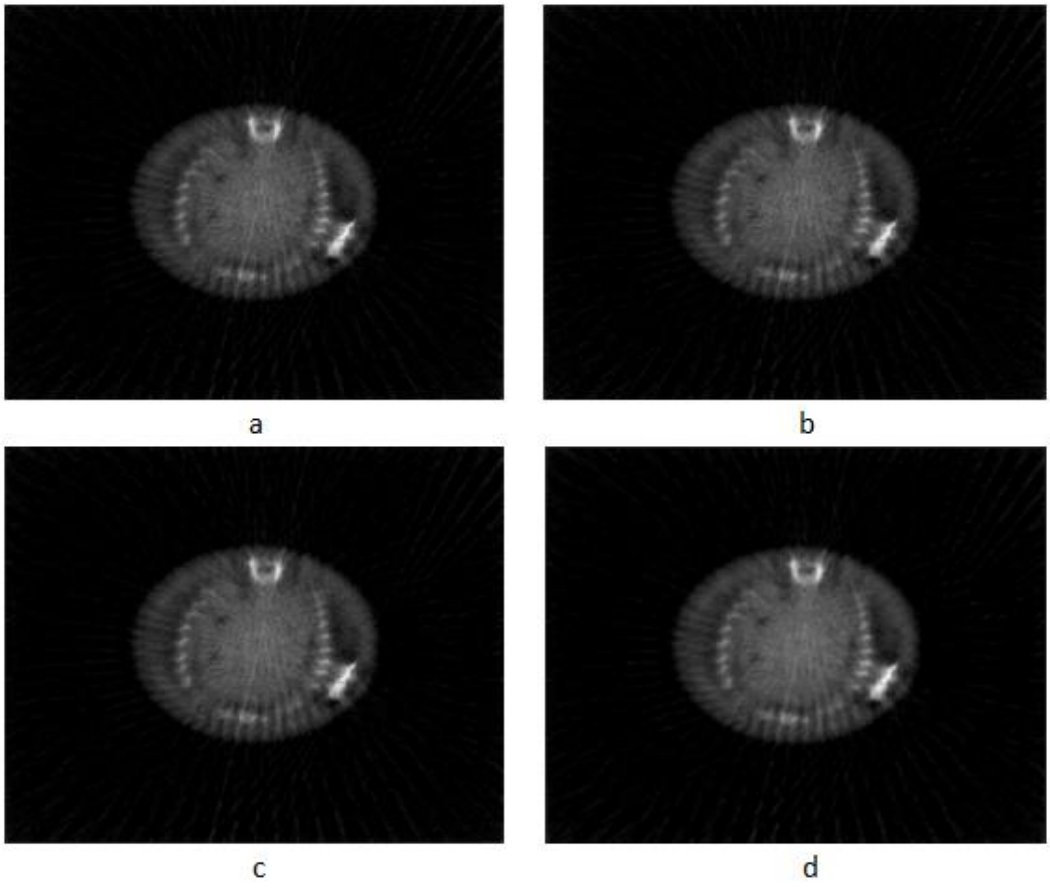


Fig 3.9 image reconstruction from projections under different $\alpha$ values using ART, 500 iterations: in image a, $\alpha = 0.001, \beta = 0.002$ ; in image b, $\alpha = 0.01, \beta = 0.002$ ; in image c, $\alpha = 0.1, \beta = 0.002$; in image d, $\alpha = 1, \beta = 0.002$.

Fig 3.9 shows the effect of another parameter, $\alpha$, in equation (47). Variable $\alpha$ determines the amount of high frequency details, shown as those projection lines, image edges, bone details and noise in the image. When $\alpha$ is large, high frequency details will miss in the image, like image d shows, image seems blurrier; when $\alpha$ is small, high frequency detail will keep which means noise is also not removed, that is not desirable to the image reconstruction. Thus, it is important to select an appropriate $\alpha$ for image reconstruction and in Fig 3.9, when $\alpha$ equals to 0.001 and 0.01, both of their reconstructed images show a great work in reconstruction. Thus, we need to work further to find out the tiny difference.

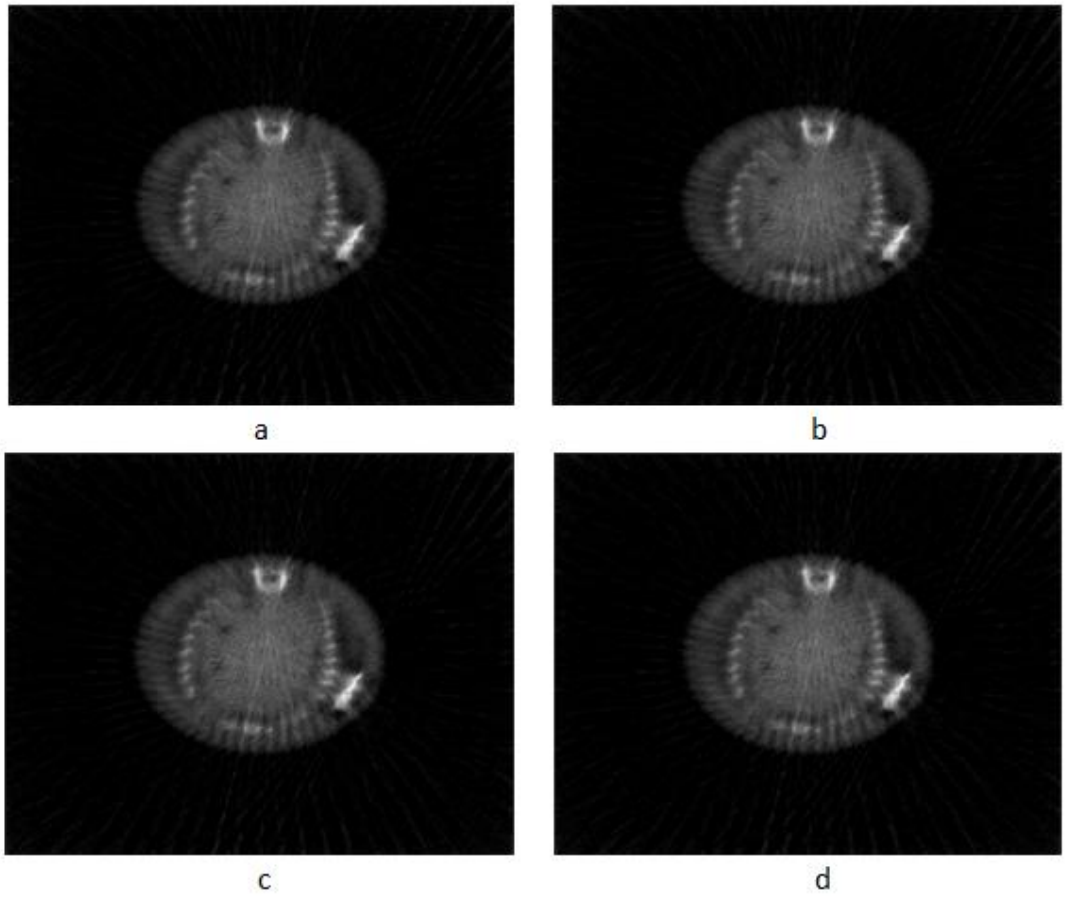

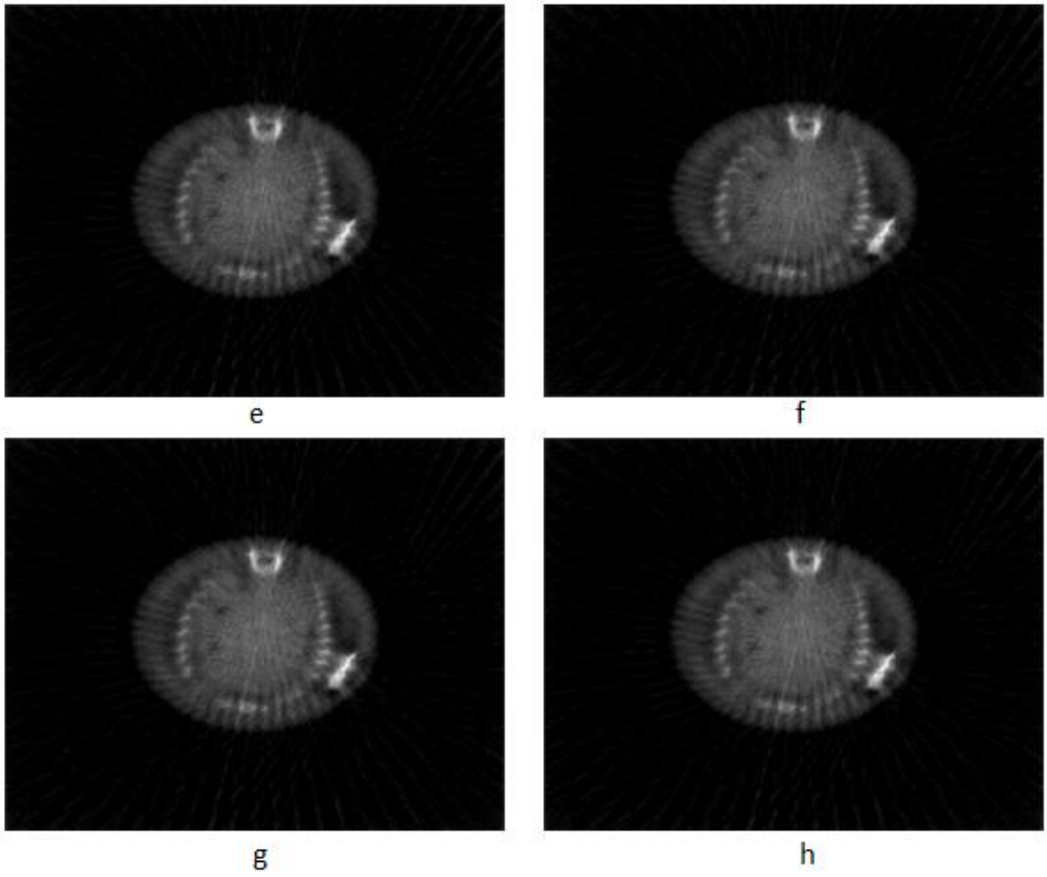


Fig 3.10 further step of image reconstruction from projections under different $\alpha$ values using ART, 500 iterations: in image a, $\alpha = 0.002, \beta = 0.002$; in image b, $\alpha = 0.003, \beta = 0.002$; in image c, $\alpha = 0.005, \beta = 0.002$ ; in image d, $\alpha = 0.007, \beta = 0.002$ ; in image e, $\alpha = 0.02, \beta = 0.002$; in image f, $\alpha = 0.03, \beta = 0.002$; in image g, $\alpha = 0.05, \beta = 0.002$; in image h, $\alpha = 0.07, \beta = 0.002$

Fig 3.10 is a further research on variable $\alpha$ and the range is among 0.001 to 0.1. From Fig 3.9, we can observe that when $\alpha$ value is small, the reconstructed image works well in removing high frequency details caused by limited projection lines. From Fig 3.10, we can see image e shows more contrast than image a in bone details. And image f also removes edge spines, better than image e. Thus, we can say $\alpha = 0.03, \beta = 0.002$ is best for image reconstruction in ART method.

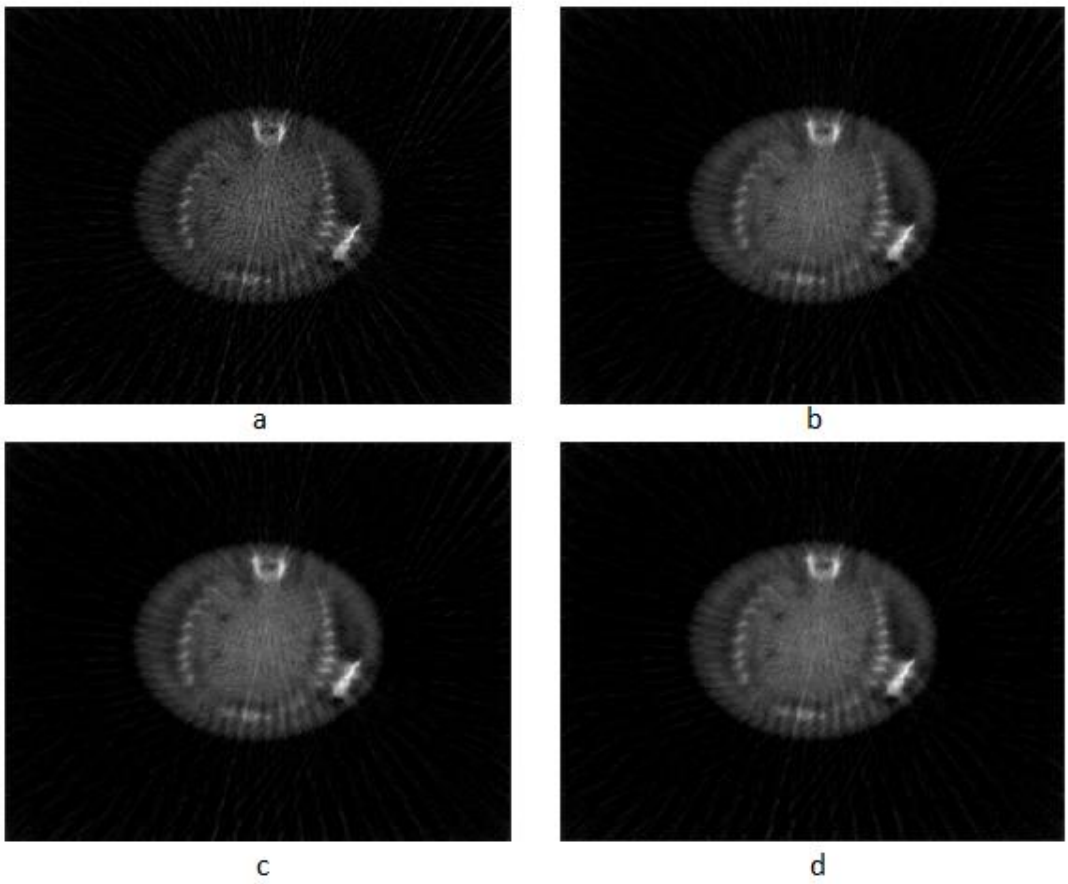


Fig 3.11 image reconstruction from projections under different iterations using ART

Compared with the original image Fig 3.6, Fig 3.11 shows the effect of iteration: with high iteration, image quality is improved. It increases the contrast and reduces the noise, those tiny points in the original image are removed, image edge artifacts are blurred. However, compared with 250 iteration and 500 iteration images, we can find they are similar, improvement of image quality is limited, hence, iteration is no necessary unlimited increasing, 500 iteration is enough.

### 3.4.3 Total Variation denoising

ART algorithm has made some progress in image enhancement, but it still cannot remove the image edge spines caused by limited projections. A further step is using TV model, x itself

variation, instead of high frequency operator L. Based on equation (52), we can also use an iterative algorithm to find the best result, assuming $\alpha = 0.03, \beta = 0.002, T = 0.001$ at first.

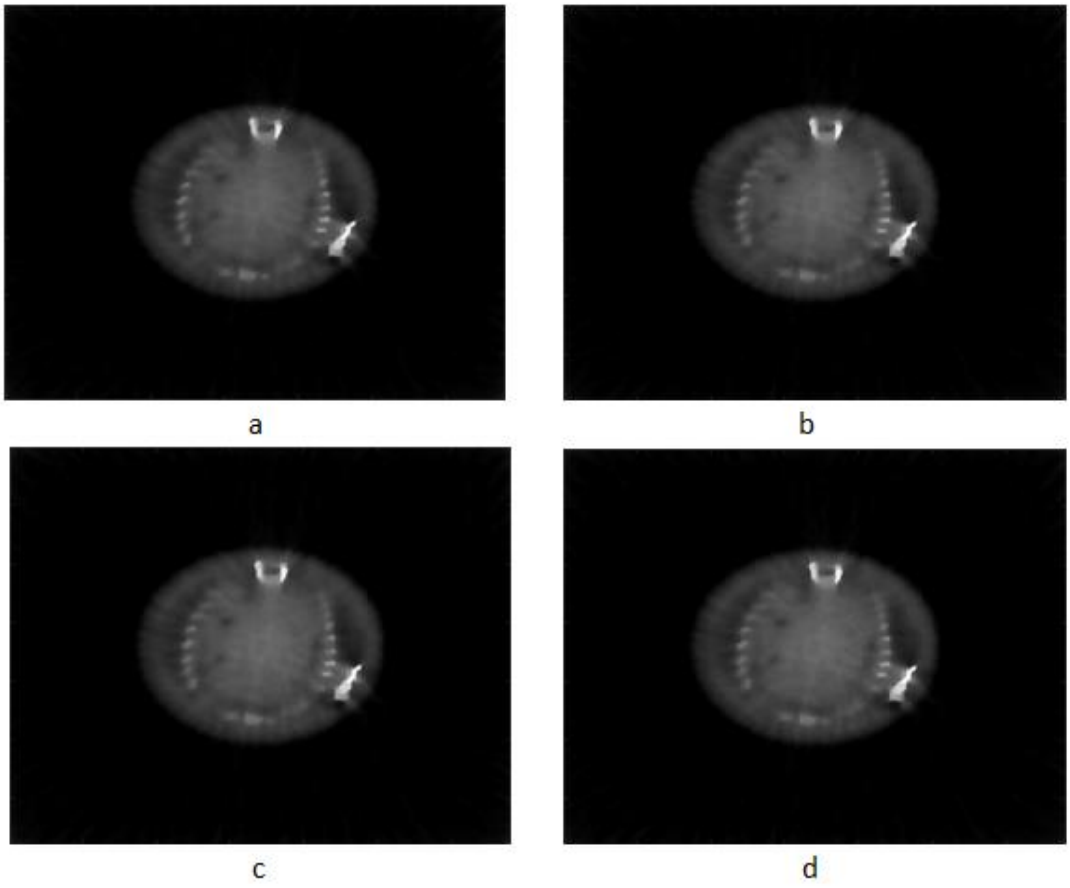


Fig 3.12 image reconstruction from projections under different $\beta$ values using TV, 500 iterations: in image a, $\alpha = 0.03, \beta = 0.001$ ; in image b, $\alpha = 0.03, \beta = 0.002$ ; in image c, $\alpha = 0.03, \beta = 0.003$; in image d, $\alpha = 0.03, \beta = 0.004$.

Fig 3.12 shows the effect of step size parameter $\beta$ in steepest descent algorithm with TV model. It determines the increment size of x every iteration, which is shown as contrast in the image. From Fig 3.12, image c, $\alpha = 0.03, \beta = 0.003$ shows the best result.

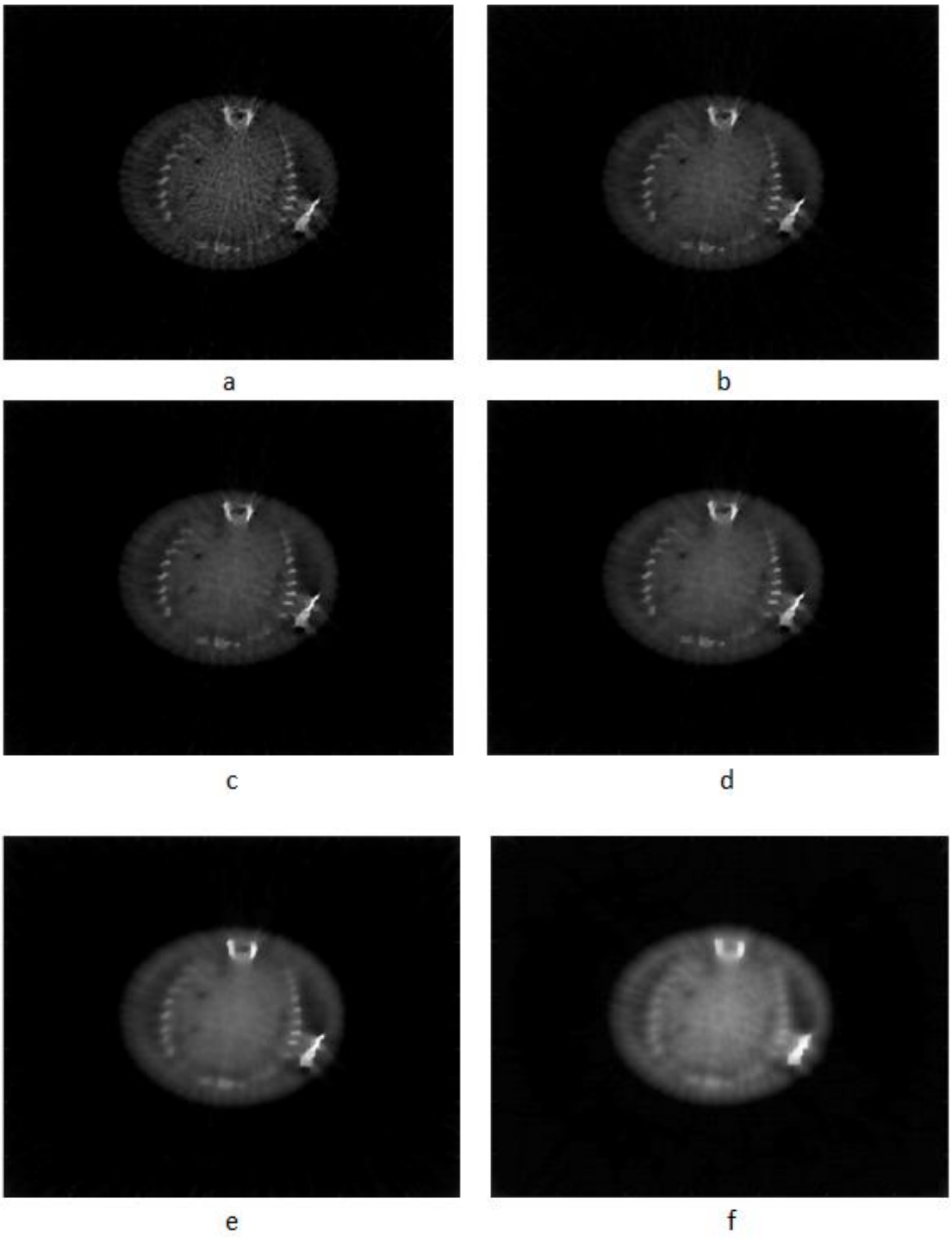


Fig 3.13 image reconstruction from projections under different $\alpha$ values using TV, 500 iterations: in image a, $\alpha = 0.001, \beta = 0.003$ ; in image b, $\alpha = 0.005, \beta = 0.003$ ; in image c,

$\alpha = 0.007, \beta = 0.003$; in image d, $\alpha = 0.01, \beta = 0.003$; in image e, $\alpha = 0.03, \beta = 0.003$; in image f, $\alpha = 0.1, \beta = 0.003$.

Fig 3.13 shows the effect of variable $\alpha$ in total variation algorithm, aiming to decrease image itself total variation in the image. From 3.13, we can observe that image d, $\alpha = 0.01, \beta = 0.003$, has the best result in this image group, reducing the high frequency noise whilst keeping the contrast.

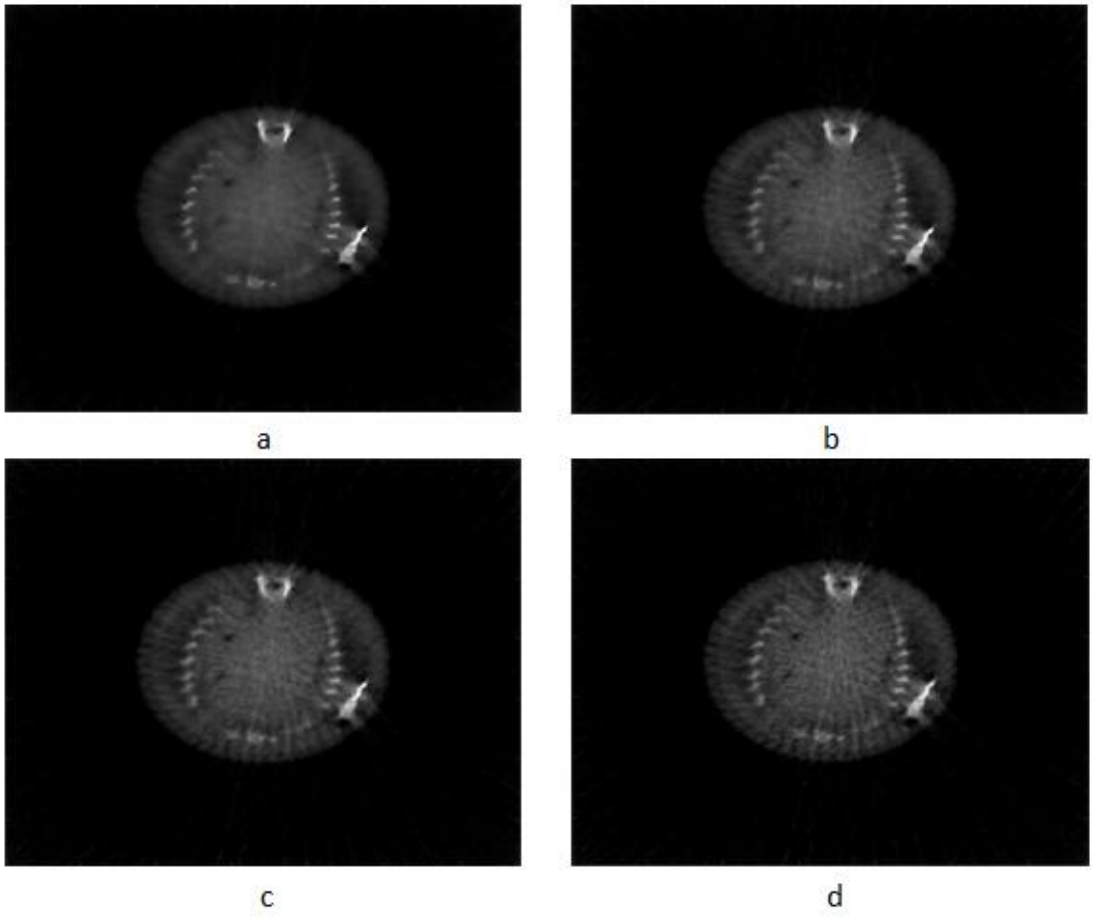


Fig 3.14 image reconstruction from projections under different $T$ values using TV, 500 iterations: in image a, $T = 0.001$; in image b, $T = 0.003$; in image c, $T = 0.005$; in image d, $T = 0.1$.

Fig 3.14 shows the effect of threshold value T in total variation algorithm. And we can see that when T increases, those tiny noise points appear again in the reconstruction image, so as the edge spines. Image becomes noisy as T grows. Thus, T should be small in TV algorithm to obtain a good result and in Fig 3.11, we can see T=0.001 provides the best result. Hence, in TV algorithm, the best parameter values are $\alpha = 0.01, \beta = 0.003, T = 0.001$

## 3.5 3D Reconstruction

The algorithm above works on each slice image of the object separately. Since it involves changing the image information, this may affect the continuity of the estimated object perpendicular to the slices. Hence, we need to consider image processing in 3D mode, removing the noise and maintaining the continuity of the object simultaneously. Therefore, we investigated 3D rendering.

### 3.5.1 ART in 3D Mode

One approach to 3D image reconstruction is to use a 3D ART algorithm, an improvement of the original ART algorithm made by replacing the Laplacian operator by a 3D one. The reconstruction result is shown in the Fig 3.13.

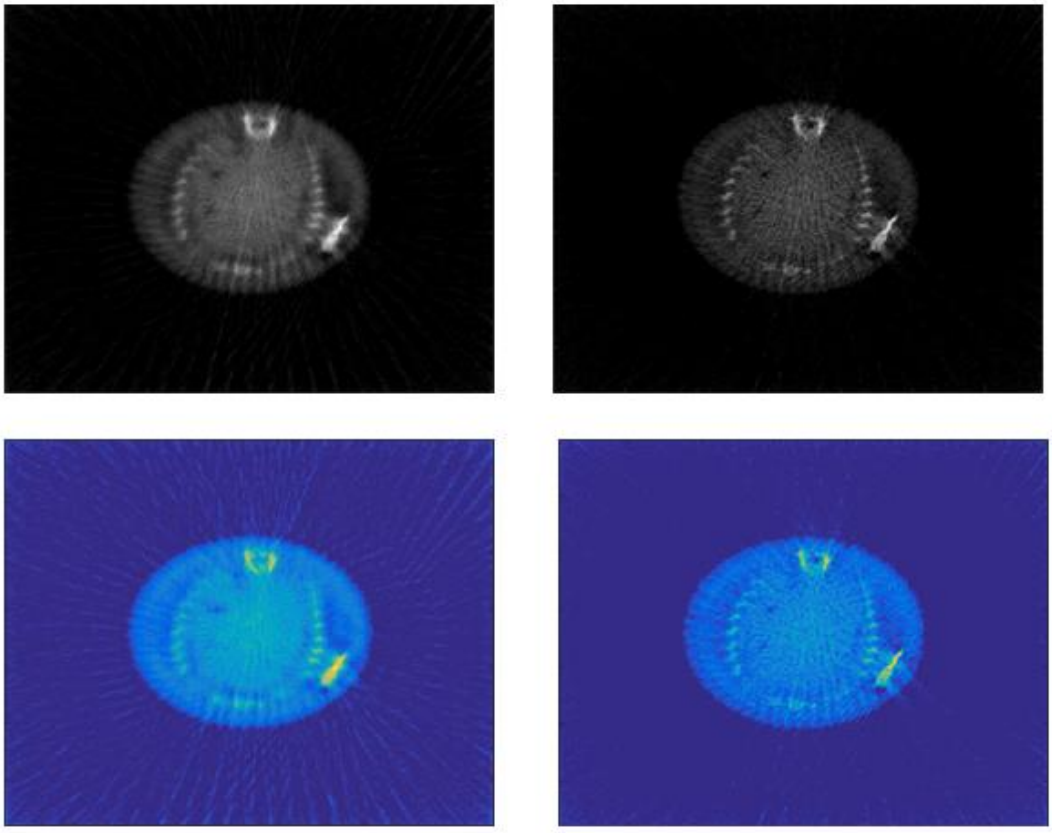

Fig 3.13 same slice image of object reconstructed in ART and 3D ART algorithm

From the grayscale image in Fig 3.13, it is hard to distinguish any difference between the two images; both of them present the details well. Thus, we transform them into another colormap, shown in the bottom row. Then we can see that 3D rendering has done a better job in reducing noise. Most of cross lines in the image caused by limited projections are removed. Hence, we can say 3D ART algorithm has made some progress in the image processing.

### 3.5.2 Total Variation in 3D

From Section 3.4, we know that TV denoising process also works well in noise removal. Therefore, we investigate whether TV can improve the results in a fully 3D reconstruction.

Based on equation (42), we define a 3D Total Variation as

$$\|\Delta(x)\| = \sum_{i,j,k}\{\varphi_T(x_{i+1,j,k} - x_{i,j,k}) + \varphi_T(x_{i,j+1,k} - x_{i,j,k}) + \varphi_T(x_{i,j,k+1} - x_{i,j,k})\} \quad (58)$$

$$\varphi_T(x) = \begin{cases} |x| - \dfrac{T}{2}, & |x| > T \\ \dfrac{1}{2T}x^2, & |x| \le T \end{cases}$$

Then taking 3D variable x and $\|\Delta(x)\|$ into equation (51), we can obtain an approximate TV denoising algorithm in three dimensional space. The result is shown in Fig 3.13

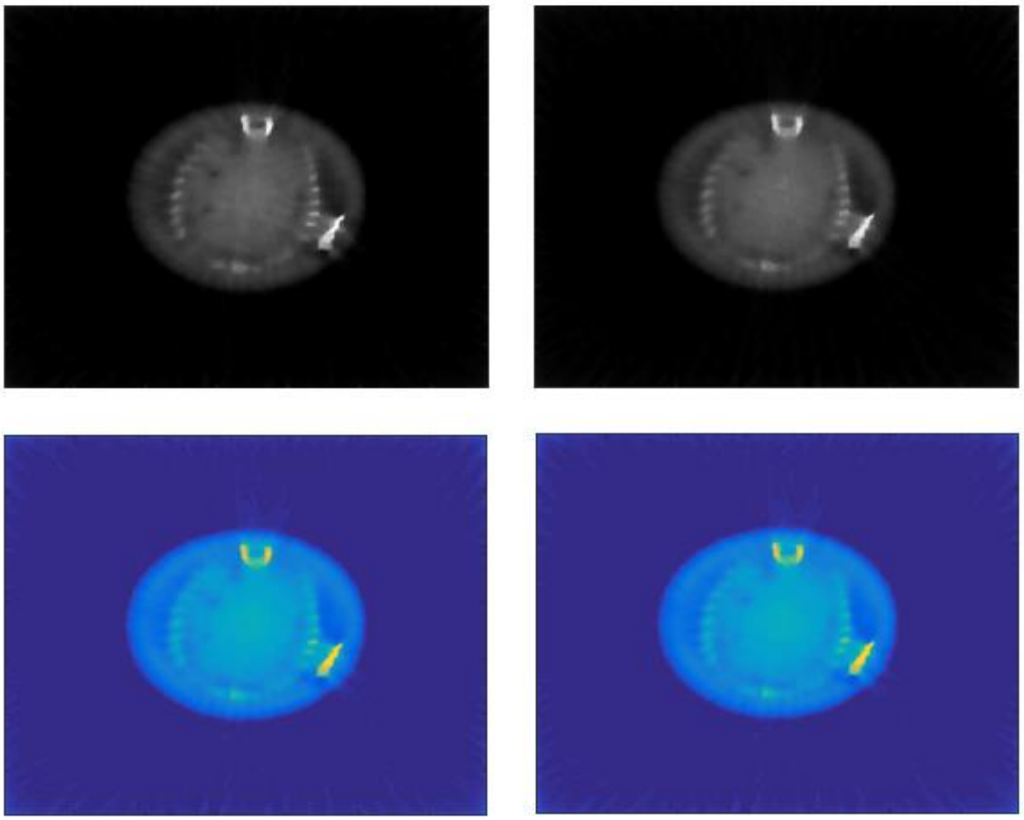

Fig 3.14 same slice image of object reconstructed in TV and 3D mode TV algorithm

From Fig 3.14, we can see the result of applying 3D TV algorithm appears very close to the single slice reconstruction image no matter in which colormap. An advantage of 3D TV

algorithm is its rendering image seems smoother than 2D slice reconstruction image, especially at object's edge side, artifacts are removed clearly. That is a great improvement in image quality recovery, thus, we can be sure that 3D rendering is very important in image processing when our interest is an object not just an image. The continuity of whole object really matters.

### 3.5.3 3D Reconstruction

Based on section 3.5.1 and section 3.5.2 work, we have created two 3D reconstruction algorithms. To explore their performance, we can use 3D Slicer software to reconstruct 3D models and their results are shown in Fig 3.14.

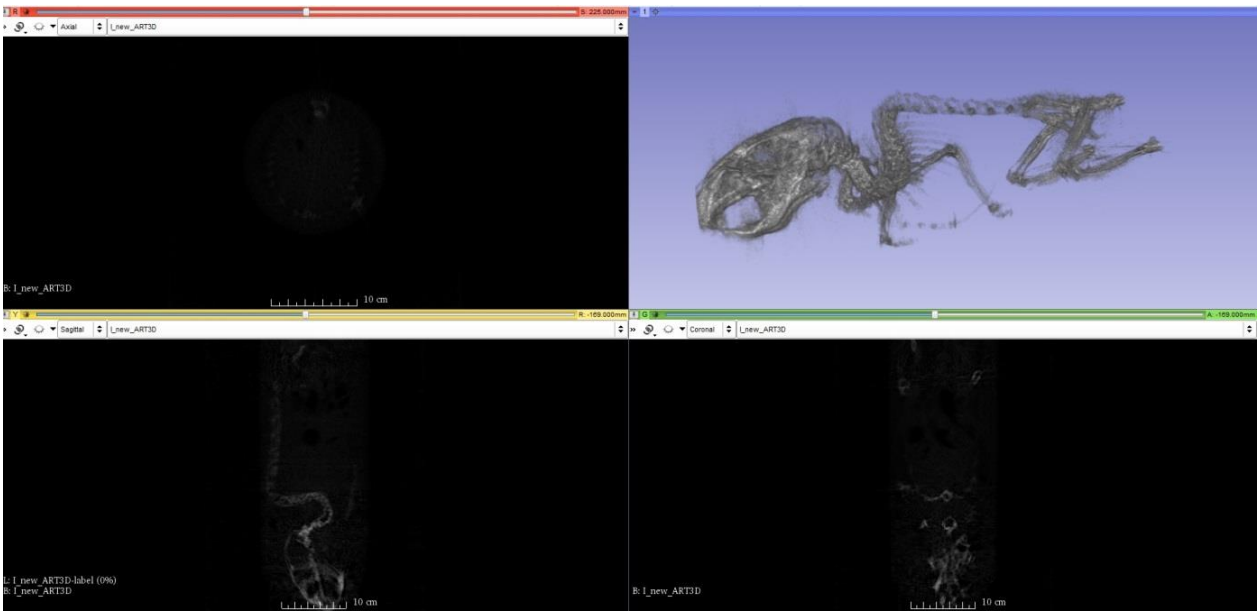

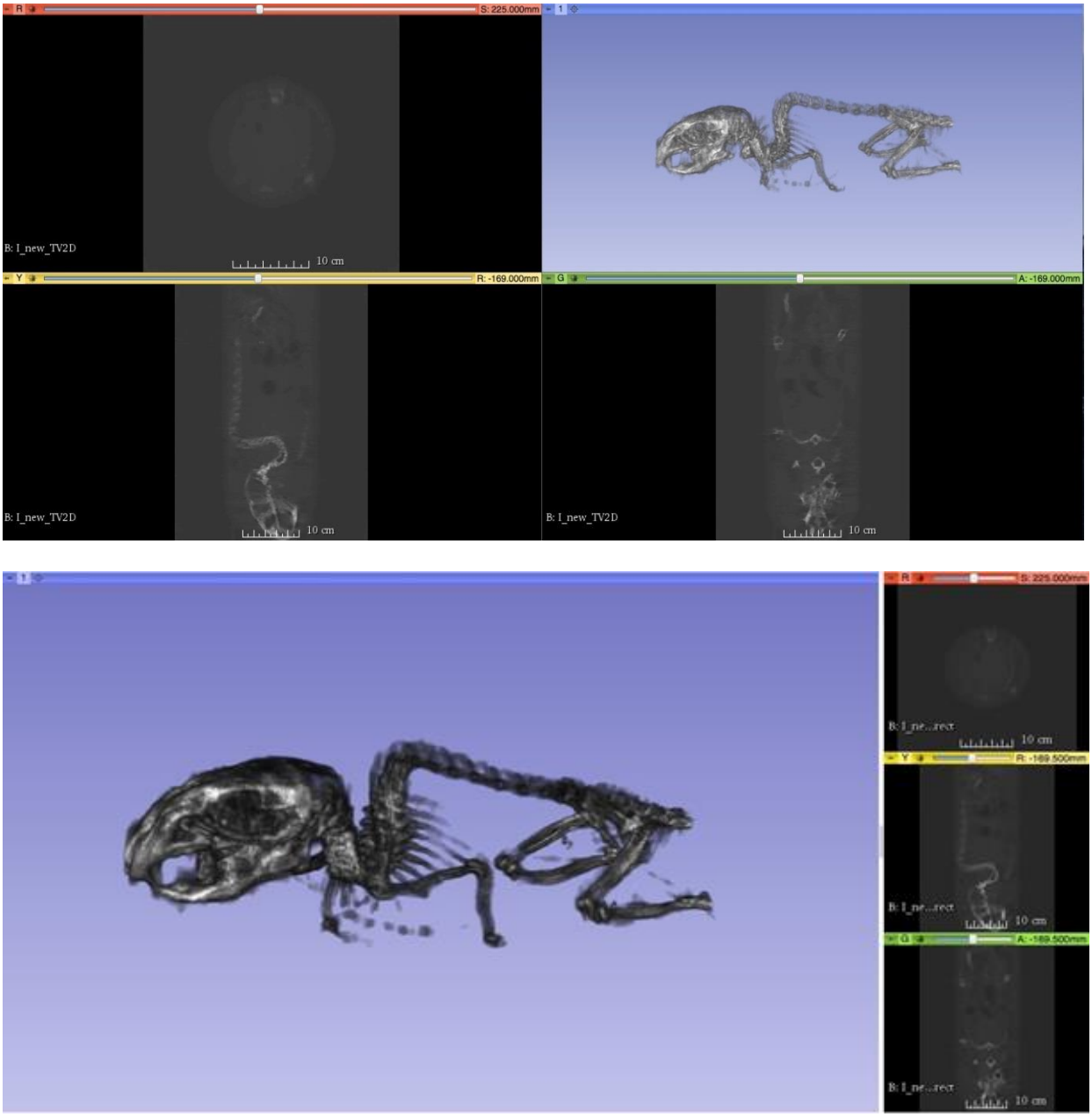


Fig 3.14 3D model rendering based on ART 3D mode algorithm, slice TV algorithm and Total Variation 3D mode algorithm: upper model is rendered from ART 3D mode algorithm, middle one is rendered from slice TV algorithm, bottom one is rendered from TV in 3D

Fig 3.14 shows the comparison between three 3D models rendered from three different algorithms. From the image, we can observe that all of them present the outline of mouse bone

structure, and models rendered from ART 3D and slice TV algorithms can show more details, including mice fingers. From the image, especially head part, we could find an amazing result that 3D model reconstructed from normal TV algorithm has the best presentation of the details and its model seems “cleaner” than the others, however, if we look at the noise, artifacts and spines, around the mouse, model rendered from 3D mode TV algorithm seems better. Thus, due to their different properties, we cannot make a judgement which method is better, but all of them is a good start in exploring 3D rendering field. And it shows the possibility of an application that 3D reconstruction from the IVIS Lumina XR system.

# Chapter 4 Conclusion

## 4.1 Conclusion

Throughout all experiments, we could find that the most important factor in image reconstruction is the number of projections; the more projections, the better the reconstructed image is. Some fundamental image processing method like interpolation can do a good job in a high density, simple structure image, like wire slice image. But for a complicated image, its improvement is limited; even worse, interpolation will destroy original image information. The best result we got is using our own designed algorithm, a combination of TV model with steepest descent ART method, to recover a reconstructed image. It increases the contrast, blurs the spines caused by limited projections, and simultaneously saves the original image information. In contrast to processing a phantom image, in the real-data case, image processing should consider more situations, including measurement error, all kinds of noise, continuity of the whole object and so on. In this work, 3D models are obtained from the volume reconstructions. Good results were obtained; the rendered model shows many details of the mouse, even its fingers. To improve 3D model, firstly, we can obtain more projections for accurate reconstruction; secondly, we can develop some more sophisticated algorithms, concentrating on volume noise removal; thirdly, we can do some detail adjustment in 3D slicer when learning the software better. Our work is a great start in 3D model rendering, but if we want to step further, it requires more time.

Reference:

[1] https://en.wikipedia.org/wiki/CT_scan, 2016, April 7

[2] Gabor T. Herman, Image reconstruction from projections, the fundamentals of computerized tomography, 1980

[3] IVIS Lumina XR Real-Time Bioluminescence, Fluorescence & X-Ray Imaging System, System Manual, 2009, Oct.

[4] Pieper S, Halle M, Kikinis R, 3D SLICER, Proceedings of the 1st IEEE International Symposium on Biomedical Imaging: From Nano to Macro 2004, vol.1, pp, 632-635.

[5] G.T. Herman, Image reconstruction from projections, Implementation and Application, Topics in Applied Physics, 1979, vol. 32,

[6] T. Saito, H. Kudo, High quality CT image reconstruction from a small number of projections, IEEE conference publication, 1988, vol. 2, pp,1272-1275,

[7] Shangkai Gao, Imaging system in medicine, 2000

[8] Shi BY, Wang C, Chen SH, et al, A novel method of CT reconstruction filter function design, CT Theory and Applications, 2010, vol. 19, No. 4, pp, 35-43.

[9] https://en.wikipedia.org/wiki/Gradient_descent, 2016, April 7

[10] https://en.wikipedia.org/wiki/Total_variation_denoising, 2016, April 7

[11] Strong D, Chan T, Edge-preserving and scale-dependent properties of total variation regularization, Inverse Problems, 2003, vol. 19, pp, S165–S187.

[12] Rudin L. I., Osher S., Fatemi E, Nonlinear total variation based noise removal algorithms, Physica D, 1992, vol. 60, pp, 259–268.

[13] S. Fang, W. Wu, H. Guo, Iteratively Refined Nonlocal Total Variation Regularization for Parallel Variable Density Spiral Imaging Reconstruction, Natural Computation (ICNC), Ninth International Conference, 2013, pp, 1382~1387

[14] Y. Hu, S. Ramani, M Jacob, A fast majorize minimize algorithm for higher degree total variation regularization, Biomedical Imaging (ISBI), IEEE 10th International Symposium, 2013, pp, 326~329

[15] D. Needell, R. Ward, Near-Optimal Compressed Sensing Guarantees for Total Variation Minimization, IEEE Transaction on Image Processing, 2013, vol. 22, pp, 3941~3949

[16] Byung Gyu Chae, and Sooyeul Lee, Sparse-View CT Image Recovery Using Two-Step Iterative Shrinkage-Thresholding Algorithm, ETRI Journal Vol. 37, No. 6, Dec. 2015, pp. 1251-1258

[17] Alasdair McAndrew, Introduction to Digital Image Processing with Matlab, Asia edition, 2004